

NASA
Technical
Paper
3192

June 1992

11-37
77358

P.36

Stress Concentrations for Straight-Shank and Countersunk Holes in Plates Subjected to Tension, Bending, and Pin Loading

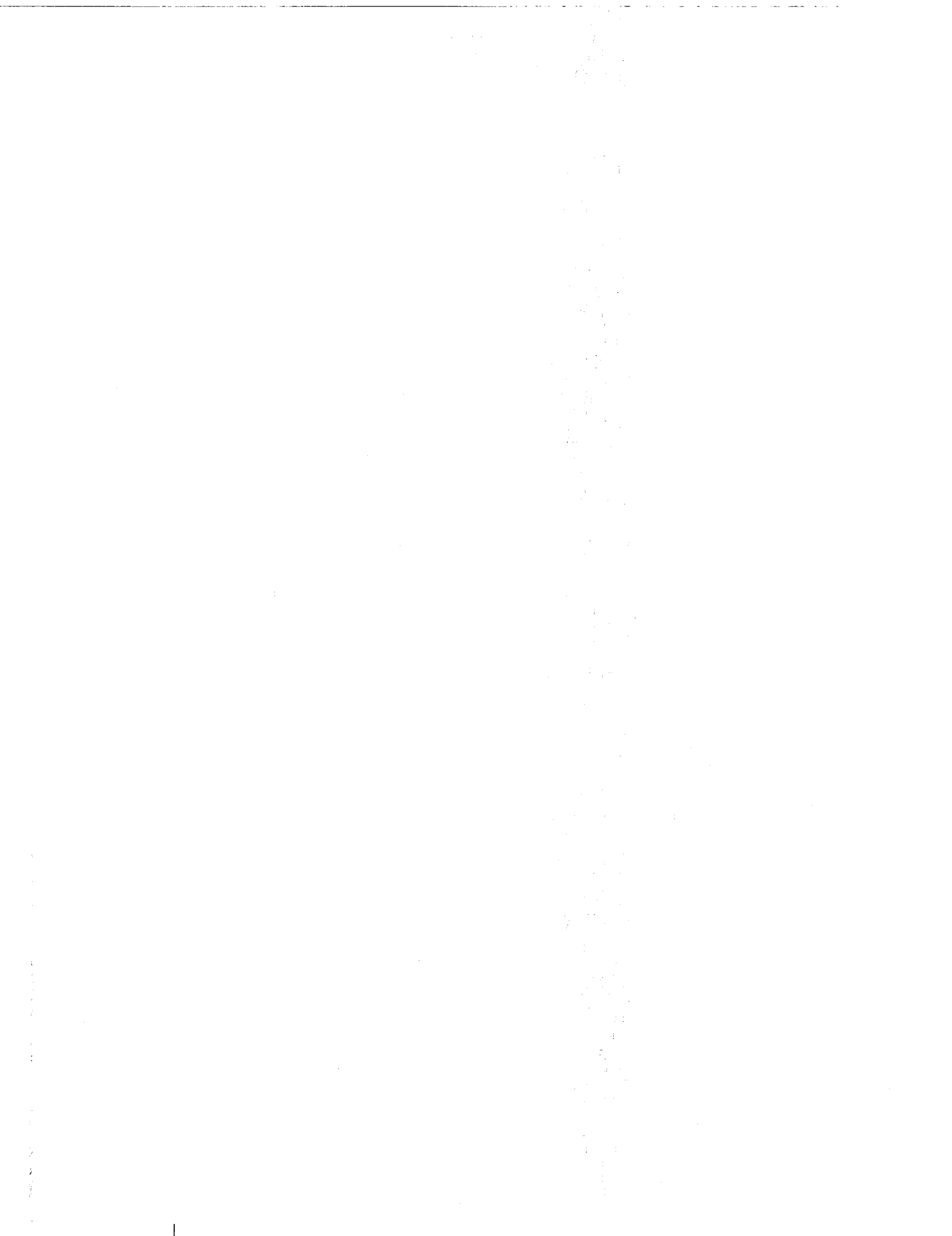
K. N. Shivakumar
and J. C. Newman, Jr.

(NASA-TP-1122) STRESS CONCENTRATIONS FOR
STRAIGHT-SHANK AND COUNTERSUNK HOLES IN
PLATES SUBJECTED TO TENSION, BENDING, AND
PIN LOADING (NASA) 36 p

N92-25997

Unclas
H1/39 0092888

The NASA logo is located in the bottom left corner of the page. It consists of the word "NASA" in a bold, sans-serif font, with a stylized "meatball" symbol to its right. The logo is partially obscured by a large, dark, textured rectangular area that covers the bottom half of the page.



**NASA
Technical
Paper
3192**

1992

**Stress Concentrations
for Straight-Shank
and Countersunk Holes
in Plates Subjected
to Tension, Bending,
and Pin Loading**

K. N. Shivakumar
Analytical Services & Materials, Inc.
Hampton, Virginia

J. C. Newman, Jr.
Langley Research Center
Hampton, Virginia



National Aeronautics and
Space Administration
Office of Management
Scientific and Technical
Information Program

Abstract

A three-dimensional stress-concentration analysis was conducted on straight-shank and countersunk (rivet) holes in a large plate subjected to various loading conditions. Three-dimensional finite-element analyses were performed with 20-node isoparametric elements. The plate material was assumed to be linear elastic and isotropic, with a Poisson's ratio of 0.3. Stress concentrations along the bore of the hole were computed for several ratios of hole radius to plate thickness (0.1 to 2.5) and ratios of countersink depth to plate thickness (0.25 to 1). The countersink angle was varied from 80° to 100° in some typical cases, but the angle was held constant at 100° for most cases. For straight-shank holes, three types of loading were considered: remote tension, remote bending, and wedge loading in the hole. Results for remote tension and wedge loading were used to estimate stress concentrations for simulated rivet or pin loading. For countersunk holes, only remote tension and bending were considered. Based on the finite-element results, stress-concentration equations were developed. Whenever possible, the present results were compared with other numerical solutions and experimental results from the literature.

Introduction

A riveted joint is a commonly used method of joining structural components. Joining introduces discontinuities (stress risers) in the form of holes, changes in the load path due to lapping, and additional loads such as rivet bearing and bending moments. Because of these changes at the joint, local stresses are elevated in the structural component. Accurate estimations of these local stresses are needed to predict joint strength and fatigue life.

Exhaustive studies on stress-concentration factors (SCF's) for holes and notches in two-dimensional (2-D) bodies subjected to a wide variety of loadings have been reported in the literature (refs. 1 and 2). Studies have also been made on three-dimensional (3-D) stress concentrations at circular holes in plates subjected to remote tension loads (refs. 3 to 6). A recent paper by Folias and Wang (ref. 6) provides a review of these previous solutions and presents a new series solution. The Folias and Wang solution covers a wide range of ratios of hole radius to plate thickness. The stress concentration at a hole in a plate subjected to bending was first presented by Neuber (ref. 4) using the Love-Kirchhoff thin-plate theory (ref. 7). Reissner (ref. 8) rederived the plate solution including the effect of shear deformation and showed that Neuber's solution was unconservative. Reissner's SCF solution for bending loads is presented in

terms of Bessel functions. Naghdi (ref. 9) extended Reissner's analysis to elliptical holes using Mathieu's functions. Rubayi and Sosropartono (ref. 10) conducted 3-D photoelastic measurements to verify Reissner's circular hole and Naghdi's elliptical hole solutions. Many other analytical (e.g., refs. 11 and 12) and experimental (e.g., refs. 13 to 15) results are reported in the literature for remote loading, but none consider 3-D effects for rivet loading in the hole.

Only two papers in the literature report results on stress concentration at countersunk holes (refs. 16 and 17). Both papers use the 3-D photoelastic slice method to obtain stress concentrations for holes in thick plates. Cheng's results (ref. 17) include stress-concentration factors for both tension and bending loads.

Three-dimensional stress concentrations at riveted joints are not fully understood. Knowledge of 3-D stress concentrations is needed to verify the adequacy of 2-D solutions in the handbooks. Furthermore, 3-D stress concentrations are needed to predict the strength and life of joints. Countersunk-rivet construction is commonly used in aircraft industries to achieve aerodynamically smooth surfaces. These joints are not amenable to 2-D approximation, and stress concentrations for countersunk holes have not been reported in handbooks.

The objective of the present study is to conduct a comprehensive analysis of three-dimensional stress concentrations for circular straight-shank and countersunk (rivet) holes in a large plate subjected to various loads encountered in structural joints. Three types of loading, remote tension, remote bending, and wedge loading in the hole (simulated pin loading), are considered for the straight-shank hole. Two types of loading, remote tension and remote bending, are considered for countersunk holes.

Three-dimensional finite-element (F-E) stress analyses of large plates with straight-shank and countersunk circular holes were conducted with the FRAC3D F-E code. The FRAC3D code is an elastic and elastic-plastic fracture mechanics code developed at NASA Langley Research Center for the analysis of cracked isotropic or anisotropic solids, based on the 20-node isoparametric element. A wide range of hole sizes (ratio of hole radius to plate thickness) and countersink depths (ratio of countersink depth to plate thickness) are considered in the analysis. The plate material is assumed to be linear elastic and isotropic, with a Poisson's ratio of 0.3. The influence of the countersink angle on stress concentrations is also examined. With the F-E results, simple, series-type stress concentration

equations are developed for a wide range of hole-radius-to-plate-thickness ratios and for any location along the bore of the hole. Whenever possible, the present results are compared with results from the literature.

Nomenclature

b	depth of straight-shank portion of hole
FEM	finite-element method
h	one-half height of plate
K_b	stress-concentration factor along bore of hole under bending
$K_{b_{\max}}$	maximum stress-concentration factor along bore of hole under bending
K_p	stress-concentration factor along bore of hole under pin loading
K_t	stress-concentration factor along bore of hole under tension
$K_{t_{\max}}$	maximum stress-concentration factor along bore of hole under tension
K_w	stress-concentration factor along bore of hole under wedge loading
M	applied remote bending moment
P	applied pin or wedge loading
r	radius of straight-shank portion of hole
S	applied remote tension stress
t	plate thickness
w	one-half width of plate
x, y, z	Cartesian coordinate system
α_{ij}	coefficients in stress-concentration equations
β_{ij}	coefficients in stress-concentration equations
θ_c	countersink angle
σ_{yy}	hoop stress at $\phi = 90^\circ$
ϕ	angle defining applied stress distribution in hole

Rivet Hole Configurations

Two types of rivet hole configurations, straight-shank and countersunk holes in a large plate, were considered. The two types of holes and nomenclature used are shown in figure 1. In the plate with a

countersunk hole, the thickness was divided into two sections: the cylindrical section, referred to as the straight-shank depth b , and the conical section, referred to as the countersink depth $t-b$. The two sections meet to form an edge referred to as the countersink edge. The stress concentrations depend on the length of the straight-shank or countersink depth. The two extreme cases of countersunk holes are when $b = 0$ (knife edge) and $b = t$ (straight-shank hole). The countersink angle was θ_c . (See fig. 1(b).)

In the present study, the plate width and height were selected large enough so that the stress-concentration solutions were not greatly affected by the remote boundaries. Stress concentrations for finite-size plates have to be generated with the use of either analytical or numerical methods. A wide range of values for hole-radius-to-plate-thickness ratio r/t and straight-shank-depth-to-plate thickness ratio b/t were considered in generating the data base on stress-concentration solutions. For the straight-shank hole, six values of r/t (encompassing the range of structural configurations used in industry) were selected: 2.5, 1.5, 1.0, 0.5, 0.25, and 0.1, with $w/r = 5$ and $h/r = 5$. For the countersunk-hole configuration, r/t values selected were 2.0, 1.0, 0.5, and 0.25 and b/t values were 0, 0.25, 0.50, and 0.75 with $w/r = 7.5$ and $h/r = 7.5$. Although the straight-shank hole configuration is a special case of the countersunk hole ($b/t = 1$), for convenience the two configurations are considered separately.

Loading Conditions

Figure 2(a) shows the three types of loadings that were applied to the plate with the straight-shank hole: remote tension stress S , remote bending moment per unit width M , and wedge loading P . Appendix A explains how the stress concentrations for a pin-loaded hole were approximated from the remote tension and wedge loading solutions. The wedge loading was imposed on the hole boundary as a normal pressure loading that has a cosine distribution and is assumed to be constant through the plate thickness. The surface pressure is defined as $(2P/\pi r t) \cos \phi$ (refs. 18 and 19) and was applied over the angle $\phi = \pm 90^\circ$. The angle ϕ is measured from the y -axis. (See fig. 2(a).) The bending moment M was applied as an equivalent remote stress that varies linearly through the plate thickness. For countersunk holes, two loading types, remote tension and remote bending, were considered. (See fig. 2(b).) Because of the lack of understanding of 3-D load transfer between the rivet and the countersunk hole, rivet (pin) loading was not considered in the current study.

Definition of Stress-Concentration Factor

Although the definition of the stress-concentration factor is given in many classical books on theory of elasticity and in stress-concentration handbooks, many of these solutions are associated with 2-D configurations. For 3-D configurations, however, the stress concentration varies along the structural discontinuity, such as along the bore of the hole. Herein, the stress-concentration factor is defined as the stress at any location along the bore of the hole normalized by a characteristic stress (related to applied loading). For configurations and loading conditions considered in this study, the highest stresses occurred along the bore of the hole at the intersection of the hole surface and the $y = 0$ plane. Even for the case of pin loading, the peak stresses occurred at $\phi = 90^\circ$ because the pin contact angle was assumed to be 90° . (See appendix A for details.) The stress-concentration factors for the three loading conditions are defined as follows.

Remote tension. The stress-concentration factor for tension K_t is the hoop stress σ_{yy} at $\phi = 90^\circ$ along the bore of the hole normalized by the applied remote tension stress S and is given by

$$K_t(z) = \frac{\sigma_{yy}(z)}{S} \quad (1)$$

Remote bending. The stress-concentration factor for bending K_b is the hoop stress σ_{yy} at $\phi = 90^\circ$ along the bore of the hole normalized by the remote outer-fiber bending stress $6M/t^2$ and is given by

$$K_b(z) = \frac{\sigma_{yy}(z)}{6M/t^2} \quad (2)$$

Wedge loading. The stress-concentration factor for wedge loading K_w is the hoop stress σ_{yy} at $\phi = 90^\circ$ along the bore of the hole normalized by the average bearing stress $P/2rt$ and is given by

$$K_w(z) = \frac{\sigma_{yy}(z)}{P/2rt} \quad (3)$$

Pin loading. The stress-concentration factor for pin loading K_p is obtained from a superposition of remote tension and wedge loading. (See appendix A.) The factor K_p is defined as the hoop stress σ_{yy} at $\phi = 90^\circ$ along the bore of the hole normalized by the average bearing stress $P/2rt$ and is given by

$$K_p(z) = \frac{\sigma_{yy}(z)}{P/2rt} \quad (4)$$

Finite-Element Modeling

A three-dimensional finite-element code FRAC3D developed at NASA Langley Research Center for analyzing cracked isotropic and anisotropic solids was used in this study. The code is based on the 20-node isoparametric element formulation. The stiffness matrix and the consistent load vectors were generated with the 2 by 2 by 2 Gaussian quadrature formula. The program uses a vector skyline Choleski decomposition algorithm (ref. 20) for solving matrix equations of equilibrium. The plates with the straight-shank hole and remote tension and wedge loading were symmetric about the $x = 0$, $y = 0$, and $z = 0$ planes. The remote bending was symmetric about the $x = 0$ and $y = 0$ planes and antisymmetric about the $z = 0$ plane. Because of these conditions, only one-eighth of the straight-shank hole plate was modeled. The FRAC3D code has an option to impose symmetry and antisymmetry boundary conditions. The plate with the countersunk hole was symmetric about the $x = 0$ and $y = 0$ planes; hence, one-fourth of the plate was modeled. The F-E model includes the full thickness of the plate.

Because many configurations were to be analyzed, a simple 3-D modeling procedure was developed to generate the finite-element meshes. In this procedure, a 2-D F-E mesh in the x - y plane was generated with refined elements near the hole boundary. Then the 2-D mesh was translated in the z -direction (with appropriate x - y transformation to account for the countersunk hole). Typical 3-D F-E meshes for one-eighth of a straight-shank hole in a plate and for one-quarter of a countersunk hole in a plate are shown in figure 3.

For all straight-shank hole models, the half-thickness of the plate was divided into six layers of unequal thickness. The layer thicknesses (starting from the $z = 0$ midplane) were 15, 13, 10, 6, 4, and 2 percent of the total plate thickness. The small thickness layers were used in the high-stress-gradient regions (near the free surface). The F-E model had 936 elements and 4725 nodes (14 175 degrees of freedom). For different values of r/t , the hole radius was kept constant and the plate thickness was scaled by t/r . The F-E mesh for $r/t = 1.0$ is shown in figure 3(a).

In the countersunk hole, there are three regions where the stress gradient is high: near the two free surfaces of the plate and at the countersink edge. Therefore, different through-the-thickness idealizations were used for different countersink edge locations b/t . Table 1 gives the details of the F-E idealizations used for countersunk holes with $b/t = 0$,

0.25, 0.50, and 0.75. Figure 3(b) shows a typical F-E model ($r/t = 0.25$ and $b/t = 0.50$) for one-quarter of a plate with a countersunk hole.

Comparison With Other Solutions

The present 3-D stress-concentration factors (SCF's) for the straight-shank hole are compared with Folias and Wang's solution (ref. 6) for remote tension and with Reissner's solution (ref. 8) for remote bending. Three-dimensional stress-concentration solutions for wedge loading or simulated pin loading have not been reported in the literature. For countersunk holes, the present solutions are compared with Cheng's photoelastic measurements (ref. 17) for thick plates subjected to tension and bending.

Straight-Shank Hole

Remote tension. The distribution of the stress-concentration factor K_t along the bore of the hole for remote tension is shown in figure 4 for various values of r/t . The stress concentrations are symmetric about the midplane ($z/t = 0$). (Note the expanded scale on the ordinate axis.) In all these cases, the plate width and height were selected large enough ($w/r = h/r = 5$) so that K_t values are not greatly affected by the finite plate. The SCF's for $r/t \leq 0.5$ are about 2 percent larger than Folias and Wang's (ref. 6) infinite-plate solutions for all z -values. (For clarity, results from ref. 6 are not shown in fig. 4.) Part of this difference may have been caused by the finite-size plate used in the present study. For $r/t = 0.1$, the present results show the same trend as that of the Folias and Wang solution (maximum SCF near the free surface), but the magnitude of the present results is 3 percent lower than the magnitude of their solution. It is expected that the classical value of $K_t = 3$ would be obtained for much thicker or thinner plates. From the plots of K_t for various values of r/t , two observations are made:

1. For $r/t \geq 0.5$, the maximum K_t occurs at $z/t = 0$ (midplane). For thicker plates ($r/t < 0.25$), the maximum K_t location shifts toward the free surface ($z/t = \pm 0.5$).

2. At $z/t = 0$, the K_t value appears to peak at a value of 3.22 for $r/t = 0.5$.

These two trends are consistent with crack-tip stress-intensity factors for cracks in thick plates, as observed by many investigators. (See, for example, ref. 21.) However, such a drop in K_t near the midplane ($z/t = 0$) for very thick plates was not

reported in reference 6, even for r/t as small as 0.02. The reason for not capturing this expected trend in reference 6 is unknown.

Remote bending. Figure 5 shows a comparison of maximum bending stress-concentration factor $K_{b_{\max}}$ calculated from the present analysis, from Reissner's shear deformation plate theory (ref. 8), and from Neuber's thin-plate theory (ref. 4). Because both Reissner and Neuber assumed that the stress distribution was linear through the thickness, $K_{b_{\max}}$ always occurs at $z/t = \pm 0.5$. However, the present F-E solutions show that the location of $K_{b_{\max}}$ is at $z/t = \pm 0.5$ (free surface) for thin plates ($r/t \geq 0.5$), but the maximum SCF is slightly interior from the free surface ($|z/t| < 0.5$) for thick plates ($r/t < 0.25$). (These results are shown subsequently.) In figure 5, the maximum SCF values from the F-E analysis are plotted for various values of r/t extrapolated to $r/t = 0$. (See the dashed curve.) Results for Reissner's shear deformation theory and the present results agree well with each other for $r/t > 1.5$. The difference between results for Reissner's solution and the present results for r/t less than unity is about 4 to 8 percent. Neuber's thin-plate theory, $K_b = (5 + \nu)/(3 + \nu)$, is inadequate even for $r/t = 2.5$ and produces values about 6 percent lower than those for Reissner's solution and the present results.

Countersunk Hole

Cheng (ref. 17) measured 3-D stress-concentration factors for countersunk holes in thick plates using a photoelastic slice technique for both tension and bending. Cheng's photoelastic models for tension (model 7) and for bending (model 8) were analyzed through the generation of separate F-E meshes. The geometric parameters of models 7 and 8 are given in table 2. For both models, $b/t = 0.6$ and $\theta_c = 90^\circ$. The SCF's for the two configurations at the critical locations are presented in table 2. The F-E results show that the maximum SCF for remote tension occurs slightly away from the countersink edge and in the straight-shank portion of the hole (at $z/t = 0.08$, whereas the countersink edge is at $z/t = 0.1$). The maximum SCF calculated from the F-E analysis is within 3 percent of Cheng's measured value. (See table 2; note that percent error is defined as the difference between solutions divided by the largest stress-concentration value.) For bending, three locations on the hole ($z/t = -0.5, 0.1, \text{ and } 0.5$) were considered for comparison. The difference between Cheng's measurements and the present solution is about 2.5 percent at $z/t = -0.5$, but the difference

is about 8 percent at the countersink edge ($z/t = 0.1$) and along the countersink flank ($z/t = 0.5$). As previously observed for straight-shank holes in thick plates, the maximum SCF is not at the free surface ($z/t = -0.5$) but is slightly interior to the free surface ($z/t = -0.48$). The drop in SCF at the free surface is attributed to the well-known free-boundary-layer effect (refs. 21 and 22).

Effect of Countersink Parameters on SCF

The two parameters that can influence the SCF for countersunk rivet holes are the countersink angle θ_c and the countersink depth $t - b$. (See fig. 1(b).) The effects of these two parameters on SCF at countersunk holes in plates subjected to tension and bending were analyzed.

Countersink Angle

The effect of small variations in the countersink angle θ_c on tension and bending SCF was analyzed with Cheng's model 7 configuration (ref. 17). Figure 6 shows the distribution of K_t and K_b along the bore of the hole for $\theta_c = 80^\circ$, 90° , and 100° . A change in θ_c of $\pm 10^\circ$ from the reference angle of 90° changes maximum K_t by about 3.5 percent at the countersink edge. However, the variation in K_t is much smaller at all other locations on the hole boundary. For the $\pm 10^\circ$ variation in θ_c , K_b varies less than 1 percent. (See fig. 6(b).) These results are for a thick plate, where $r/t = 0.24$. For thin plates, used in aircraft applications (r/t of about 2), the effect of θ_c variation on SCF is of the same order as that shown for the thick plates.

Countersink Depth

As previously mentioned, the countersink-depth-to-plate-thickness ratio is defined as $1 - (b/t)$, where b/t represents the ratio of the straight-shank depth to the plate thickness. For convenience, b/t is used as a depth parameter. Figure 7 shows the distribution of K_t and K_b along the bore of the hole ($-0.5 \leq z/t \leq 0.5$) for $b/t = 0, 0.25, 0.50$, and 0.75 . The plate $w/r = h/r = 7.5$, $r/t = 2.0$, and $\theta_c = 100^\circ$ (a typical value for the aircraft industry). In figure 7(a), the maximum tension SCF's occur at the countersink edge for all values of b/t . However, in thick plates, the maximum SCF's occur slightly away from the countersink edge, on the straight-shank portion of the hole. The maximum tension SCF's are 4.06, 4.10, 3.82, and 3.39 for $b/t = 0, 0.25, 0.50$, and 0.75 , respectively. The highest SCF for the countersunk hole under remote tension is about 37 percent higher than the classical 2-D value ($K_t = 3$). In contrast, for

finite-thickness plates, SCF's for countersunk holes are only about 30 percent higher because the finite thickness elevates the SCF, as shown in figure 4. Figure 7(b) shows the bending SCF distribution for various values of b/t . In contrast to tension loading, the maximum bending SCF is almost unaffected by b/t , except for $b/t = 0$ (near the knife-edge location). The variation of maximum K_b (at $z/t = \pm 0.5$) is less than 1 percent for $0.25 \leq b/t \leq 0.75$. The maximum bending SCF at $z/t = -0.5$ is -2.41 for $b/t = 0$; this K_b is about 24 percent lower than that for $b/t = 0.50$. (Note that the SCF will be positive at $z/t = -0.5$ if the moment is reversed.)

Stress-Concentration Factor Equations

In this study, 3-D stress-concentration factors for a wide range of hole configurations and loadings were generated with the finite-element method. These solutions may be used in structural design as they are or they may be interpolated to calculate stress concentration at any other location along the hole boundary or for other hole (r/t and b/t) configurations. The F-E solutions will be easier to use if equations are developed. In this section, SCF equations are developed by fitting the F-E results to double-series polynomial equations. Separate equations are developed for straight-shank and countersunk holes subjected to different loading conditions.

Multiparameter least-squares equation fits were performed with the International Mathematical and Statistical Library routine QRASOS, which uses the Householder transformation for matrix factorization (ref. 23). The weight factor for each of the SCF values along the bore of the hole is selected such that the weight is proportional to the length between the two neighboring points on either side of the point under consideration. For example, a weight factor for the i th point is $(z_{i+1} - z_i)/2t$. This procedure of selecting the weight factor minimizes the area under the SCF curve on the z -axis. Also, this procedure gives good fits to even unequally spaced data points without higher order oscillations, which are generally present in a high-order polynomial fit.

Straight-Shank Hole

The configuration for a plate with a straight-shank hole is symmetric about the $z = 0$ plane. (See fig. 2(a).) The tension and the wedge loading are symmetric about the $z = 0$ plane, whereas the bending is antisymmetric about the $z = 0$ plane. Therefore, an even-power polynomial in z and a general polynomial in r/t were used to fit SCF results for tension (K_t) and for wedge loading (K_w). An

odd-power polynomial in z and a general polynomial in r/t were used to fit the SCF results for bending (K_b). The forms of the SCF equations are

$$K_m = \sum_{i=0}^4 \sum_{j=0}^4 \alpha_{ij} (r/t)^i (z/t)^{2j} \quad (5)$$

where $m = t$ for remote tension and $m = w$ for wedge loading and

$$K_b = \sum_{i=0}^4 \sum_{j=1}^4 \alpha_{ij} (r/t)^i (z/t)^{2j-1} \quad (6)$$

for remote bending. Equations (5) and (6) apply over the range $0.1 \leq r/t \leq 2.5$. The orders of the polynomials for r/t and z/t are selected by trial and error such that the maximum difference between the F-E results and the equation results is minimal and the sum of residuals is a minimum. The coefficients α_{ij} are given in tables 3, 4, and 5 for remote tension, wedge loading, and remote bending, respectively.

Figures 8 to 10 show a comparison between the F-E results and the equation results for various values of r/t for remote tension, wedge loading, and remote bending, respectively. (Note that an enlarged scale is used on the ordinate axis in figs. 8 to 10 to magnify the difference between the equation and the F-E results.) The equation results agree well with the F-E results for all values of r/t and for all three loading conditions. The maximum difference between the F-E solutions and the equation results is about 1 percent. For both remote tension (fig. 8) and wedge loading (fig. 9), the SCF drops near the free surface. The drop is larger for thicker plates (smaller r/t). The bending SCF (fig. 9) is almost linear for $r/t \geq 1.5$ and becomes nonlinear for thick plates ($r/t \leq 1.0$), particularly near the free surface. Thus, the assumption of linear stress (or strain) distribution through the thickness made in the Reissner (ref. 8) and Neuber (ref. 4) analyses is valid only for $r/t \geq 1.0$. For $r/t = 0.5$ and 0.25 , the maximum SCF is not at the free surface ($z/t = \pm 0.5$); it is located in the interior of the plate ($|z/t| < 0.5$).

Now that the SCF equations for remote tension and wedge loading have been established, the SCF equation for simulated pin loading is written as

$$K_p = \frac{K_w + (r/w)K_t}{2} \quad (7)$$

Equation (7) is restricted to $r/w = 0.2$ because K_t and K_w are generated for a plate with $r/w = 0.2$. The

development of equation (7) is given in appendix A. The results from equation (7) are shown in figure 11. Of course, these results show the same trends as those shown in figures 8 and 9 for tension and wedge loading, respectively.

Countersunk Holes

The configurations of the countersunk hole dictate that two separate SCF equations be fit: one equation for the straight-shank part ($-0.5 \leq z/t \leq (b/t - 0.5)$) and the other equation for the countersunk portion ($(b/t - 0.5) \leq z/t \leq 0.5$). Furthermore, separate equations were developed for each value of b/t . A general polynomial series equation in terms of r/t and z/t was fit to the F-E results with the least-squares procedure previously discussed. The SCF equations are given by

$$K_m = \sum_{i=0}^3 \sum_{j=0}^4 \alpha_{ij} (r/t)^i (z/t)^j \quad (8)$$

for $-0.5 \leq z/t \leq (b/t - 0.5)$ and

$$K_m = \sum_{i=0}^3 \sum_{j=0}^4 \beta_{ij} (r/t)^i \{ [z - b + (t/2)] / (t - b) \}^j \quad (9)$$

for $(b/t) - 0.5 \leq z/t \leq 0.5$. Equations (8) and (9) apply over $0.25 \leq r/t \leq 2.5$. Coefficients α_{ij} and β_{ij} for various values of b/t are given in tables 6 and 7 for remote tension and remote bending, respectively. Figures 12 and 13 show comparisons between results for equations (8) and (9) with the F-E results for remote tension and remote bending, respectively. The equation results and F-E results agree well, except near the free surface for thick plates. Even for thick plates, the maximum SCF is within 2 percent of the F-E results for all b/t values. Note that the bending SCF at $z/t = 0.5$ for the straight-shank hole ($b/t = 1.00$, see fig. 10) is slightly less than that at $z/t = -0.5$ for the countersunk hole with $b/t = 0.50$ (see fig. 13(c)).

In appendix B, a FORTRAN program is given to evaluate the SCF's for straight-shank and countersunk holes subjected to remote tension, remote bending, pin loading, and wedge loading. This program is based on equations (5) to (9) with the coefficients presented in tables 3 to 7. This program may be used to generate three-dimensional SCF's for any value of b/t and r/t and at any location along the bore of the hole. To generate the SCF's for values of b/t other than those used in this study, an interpolation scheme between the available solutions has been implemented in the program.

Concluding Remarks

A comprehensive three-dimensional stress-concentration analysis of straight-shank and countersunk (rivet) holes in a large plate subjected to various loading conditions encountered in service was conducted. The plate material was assumed to be isotropic, with a Poisson's ratio of 0.3. Three-dimensional finite-element analyses were performed with 20-node isoparametric elements. Stress-concentration factors for wide ranges of hole-radius-to-plate thickness and countersink-depth-to-plate thickness ratio were generated. The countersink angle was varied from 80° to 100° in some typical cases, but the angle was held constant at 100° for most cases. For straight-shank holes, three types of loading, remote tension, remote bending, and wedge loading, were considered; for the countersunk hole only remote tension and remote bending were considered. Series-type equations were fit to the finite-element re-

sults. These equations generally agreed within 1 percent of the finite-element results.

Tension stress-concentration factor (SCF) for a countersunk hole was about 37 percent higher than the classical (2-D) solution for a circular hole (SCF = 3); the SCF was about 30 percent higher than the 3-D SCF for a straight-shank hole with the same hole-radius-to-plate-thickness ratio. However, the bending SCF was almost unaffected by countersinking the hole, except for the knife-edge case (no straight shank). Variation in the countersink angle (80° to 100°) had little effect on the peak SCF (a change of less than 3.5 percent) for both remote tension and remote bending.

NASA Langley Research Center
Hampton, VA 23665-5225
April 15, 1992

Appendix A

Computation of Stress-Concentration Factors for a Pin-Loaded Hole in a Large Plate

This appendix shows how the SCF solutions for the wedge loading and for the remote uniform stresses can be used to predict the SCF for a pin-loaded (or rivet-loaded) plate. In this analysis, as already mentioned in the text, the pin and the plate surface are assumed to be smooth and the pin fits snugly into the hole (no clearance). Two-dimensional studies (refs. 24 to 27) have clearly demonstrated that the maximum tensile stress concentration due to pin loading occurs at the end of the contact between the pin and the hole boundary. For a snugly fit pin joint and modeling the pin, these references show that the contact angle is about 83° . However, Crews et al. (ref. 25) show that a contact angle of 83° or 90° (between the pin and the hole) has very little effect on the maximum stress concentration (about a 3-percent difference). Because the present analysis assumes that the contact angle is 90° , the maximum stress concentration occurs also at 90° . Therefore, the superposition of the wedge loading and remote loading solutions (both give the maximum stresses at 90°) give the highest stress concentration. If the contact angle is assumed to be 83° , then the maximum stress at 90° is within 3 percent of the maximum value at 83° .

In the present analysis, the pin-load reaction is approximated by a cosine distribution over the contact angle ϕ of $\pm 90^\circ$ (refs. 18 and 19). (The angle is measured from the y -axis; see fig. 2(a).) Consider a

pin-loaded hole as in the plate shown in figure 14(a), where the plate height h is large compared with the hole radius. This condition results in a uniform stress of $P/2wt$ at $y = -h$. The SCF for this problem is measured by the σ_{yy} stress at $y = 0$ and $x = r$. Consider another problem, shown in figure 14(b), where the pin load acts on the lower half of the hole and the corresponding remote stress is $P/2wt$ at $y = h$. The two problems in figures 14(a) and 14(b) are identical except that the stress is 180° out of phase. On the x -axis, the σ_{yy} stress for these two problems is identical. The sum of these two loading conditions in figures 14(a) and 14(b) can be represented as wedge loading and remote tension, as shown in figures 14(c) and 14(d). Therefore, σ_{yy} stress on the x -axis for the pin-load case is half the sum of the σ_{yy} stress due to wedge loading and remote tension. Alternatively, the stress concentration for the pin load K_p is defined in terms of the stress-concentration factor for the wedge load K_w and the remote tension load K_t as follows:

$$K_p = \frac{K_w + (r/w)K_t}{2} \quad (A1)$$

A plane strain analysis of $r/w = 0.2$ was performed with the 3-D finite-element analysis described in the text. The computed pin-load SCF from equation (A1) is $K_p = 0.994$. This solution agrees reasonably well with the experimental results (0.985) reported by Chang et al. (ref. 24). Some differences are observed between the present results and those of other analyses, such as Crews et al. (0.87, ref. 25), De Jong (1.058, ref. 26), and Eshwar et al. (0.922, ref. 27).

Appendix B

Computer Code Used To Calculate Stress-Concentration Factors

This appendix presents a FORTRAN program and subroutine (SCF3D) used to calculate the stress-concentration factor at any location along a straight-shank or countersunk hole subjected to various loadings. This program was developed such that it may be readily incorporated into other stress-analysis or life-prediction codes. The program returns K_t , K_b , K_p , and K_w for remote tension, remote bending, pin loading, and wedge loading. The simulated pin-load value K_p was calculated from K_t , K_w , and procedures that are presented in appendix A.

```
PROGRAM MAIN
C
C COMPUTES THREE-DIMENSIONAL STRESS-CONCENTRATION FACTORS FOR
C STRAIGHT-SHANK OR COUNTERSUNK HOLES SUBJECTED TO REMOTE
C TENSION, REMOTE BENDING, PIN LOADING AND WEDGE LOADING
C
CHARACTER*1 LCASE
PRINT *, 'INPUT LOAD CASE (TENSION, BENDING, PIN, WEDGE): T, B, P or W'
READ 1, LCASE
1 FORMAT(A1)
PRINT *, 'INPUT: r/t, b/t, z/t, r/w ?'
READ *, RT,BT,ZT,RW
CALL SCF3D(RT,BT,ZT,RW,LCASE,SCF)
PRINT *, 'r/t = ',RT,' b/t = ',BT,' z/t = ',ZT,' r/w = ',RW
PRINT *, 'Stress-Concentration Factor = ', SCF
STOP
END
SUBROUTINE SCF3D(RT,BT,ZT,RW,LCASE,SCF)
-----
C
C SCF3D - VERSION CREATED APRIL 1991
C
C DEVELOPED BY: Kunigal N. Shivakumar and J. C. Newman, Jr.
C
C THREE-DIMENSIONAL STRESS-CONCENTRATION IN COUNTERSUNK AND STRAIGHT
C SHANK RIVET HOLES.
C
C PARAMETERS IN THE CALL STATEMENT:
C (A) INPUT
C
C BT = b/t, STRAIGHT SHANK LENGTH TO PLATE THICKNESS RATIO
C RT = r/t, HOLE RADIUS TO THICKNESS RATIO
C ZT = z/t, LOCATION WHERE STRESS-CONCENTRATION FACTOR IS REQUIRED
C AS A RATIO OF PLATE THICKNESS
C NOTE: 'z' IS MEASURED FROM THE MID-PLANE OF THE PLATE
C RW = r/w, HOLE RADIUS TO PLATE WIDTH
C LCASE - LOADING CASE AS DEFINED BELOW
C
```

```

C          STRAIGHT SHANK
C          LCASE = T, REMOTE TENSION
C          LCASE = B, REMOTE BENDING
C          LCASE = P, PIN LOADING
C          LCASE = W, WEDGE LOADING
C
C          COUNTER SUNK HOLE
C          LCASE = T, REMOTE TENSION
C          LCASE = B, REMOTE BENDING
C
C (B) OUTPUT
C
C          SCF - THREE-DIMENSIONAL STRESS-CONCENTRATION FACTOR
C
C          REMOTE TENSION: SCF = MAX. STRESS/S
C                          S = REMOTE APPLIED STRESS
C
C          REMOTE BENDING: SCF = MAX. STRESS/(6M/(t*t))
C                          M = REMOTE APPLIED MOMENT PER
C                          UNIT WIDTH
C
C          PIN LOAD: SCF = MAX. STRESS/(P/(2rt))
C                     P = PIN LOAD
C
C          WEDGE LOAD: SCF = MAX. STRESS/(P/(2rt))
C                     P = WEDGE LOAD
C
C          NOTE: SCF FOR SIMULATED RIVET LOADING IS OBTAINED BY
C          ADDING ONE-HALF OF THE SCF FOR REMOTE TENSION
C          S = P/(2wt) AND ONE-HALF OF THE SCF FOR WEDGE
C          LOADING (2w IS TOTAL WIDTH OF PLATE).
C-----
C          CHARACTER *1, LCASE,MCASE,NCASE
C          DATA MCASE,NCASE/1HT,1HW/
C
C BEGIN ANALYSIS
C
C INPUT ERROR WHEN IERR .NE. 0 (PARAMETER OUT OF RANGE)
C          IERR = 0
C          IF(BT .LT. 0.0 .OR. BT .GT. 1.0) IERR = 1
C          IF(IERR .EQ. 1) PRINT *, 'INPUT PARAMETER b/t OUT OF RANGE'
C          IF(RT .GT. 2.5) IERR = 2
C          IF(RT .LT. .25) IERR = 2
C          IF(IERR .EQ. 2) PRINT *, 'INPUT PARAMETER r/t OUT OF RANGE'
C          IF(ZT .LT. -0.501 .OR. ZT .GT. 0.501) IERR = 3
C          IF(IERR .EQ. 3) PRINT *, 'INPUT PARAMETER z/t OUT OF RANGE'
C          IF(RW .GT. 0.25) IERR = 4

```

```
IF(IERR .EQ. 4) PRINT *, 'INPUT PARAMETER r/w OUT OF RANGE'  
IF(IERR .NE. 0) STOP
```

C

```
IF (BT .EQ. 1.0) THEN  
IF(LCASE .EQ. 'P' .OR. LCASE .EQ. 'p') GOTO 10  
CALL SSHANK(RT,ZT,LCASE,SCF)  
GOTO 20  
10 CONTINUE  
CALL SSHANK(RT,ZT,MCASE,SCFT)  
CALL SSHANK(RT,ZT,NCASE,SCFW)  
SCF = (SCFW + RW * SCFT) * 0.5  
20 RETURN  
ELSE  
IF (BT .EQ. 0.0) THEN  
CALL CSHANK(RT,BT,ZT,LCASE,SCF)  
RETURN  
ENDIF  
IF(BT .GT. 0.0 .AND. BT .LE. 0.25) THEN  
CALL NZT(BT,ZT,0.0,0.25,ZT1,ZT2)  
CALL CSHANK(RT,0.0,ZT1,LCASE,SCF1)  
CALL CSHANK(RT,0.25,ZT2,LCASE,SCF2)  
SCF = SCF1 + (SCF2-SCF1)/0.25 * BT  
RETURN  
ENDIF  
IF(BT .GT. 0.25 .AND. BT .LE. 0.5) THEN  
CALL NZT(BT,ZT,0.25,0.5,ZT1,ZT2)  
CALL CSHANK(RT,0.25,ZT1,LCASE,SCF1)  
CALL CSHANK(RT,0.50,ZT2,LCASE,SCF2)  
SCF = SCF1 + (SCF2-SCF1)/0.25 * (BT-0.25)  
RETURN  
ENDIF  
IF(BT .GT. 0.50 .AND. BT .LE. 0.75) THEN  
CALL NZT(BT,ZT,0.5,0.75,ZT1,ZT2)  
CALL CSHANK(RT,0.50,ZT1,LCASE,SCF1)  
CALL CSHANK(RT,0.75,ZT2,LCASE,SCF2)  
SCF = SCF1 + (SCF2-SCF1)/0.25 * (BT-0.50)  
RETURN  
ENDIF  
IF(BT .GT. 0.75 .AND. BT .LT. 1.0) THEN  
CALL NZT(BT,ZT,0.75,1.0,ZT1,ZT2)  
CALL CSHANK(RT,0.75,ZT1,LCASE,SCF1)  
CALL SSHANK(RT,ZT,LCASE,SCF2)  
SCF = SCF1 + (SCF2-SCF1)/0.25 * (BT-0.75)  
RETURN  
ENDIF
```

```

ENDIF
END
SUBROUTINE NZT(BT,ZT,BT1,BT2,ZT1,ZT2)
C
C EVALUATE APPROPRIATE Z-LOCATION FOR COUNTER-SUNK HOLE
C
IF(ZT .GT. (BT-0.5) .AND. ZT .LE. 0.5) THEN
ZT1 = BT1-0.5 + (ZT-BT+0.5) * (1.-BT1)/(1.-BT)
ZT2 = BT2-0.5 + (ZT-BT+0.5) * (1.-BT2)/(1.-BT)
ELSE
ZT1 = BT1-0.5 + (ZT-BT+0.5) * BT1/BT
ZT2 = BT2-0.5 + (ZT-BT+0.5) * BT2/BT
ENDIF
RETURN
END
SUBROUTINE SSHANK(RT,ZT,LCASE,SCF)
C-----
C
C THREE-DIMENSIONAL STRESS-CONCENTRATION EQUATION FOR STRAIGHT
C SHANK RIVET HOLE SUBJECTED TO:
C (1) REMOTE TENSION
C (2) REMOTE BENDING
C (3) PIN LOADING IN HOLE (r/w < 0.25)
C (4) WEDGE LOADING IN HOLE
C
C RANGE OF PARAMETERS: -0.5 < z/t < 0.5; 0.25 < r/t < 2.5
C-----
DIMENSION ALP(4,5,2), ALPB(4,4)
CHARACTER *1, LCASE
DATA ALP/
1 3.1825, .1679, -.2063, .0518,
2 .4096, -1.5125, 1.1650, -.2539,
3 -1.2831, 2.8632, -2.0000, .4239,
4 2.2778, -6.0148, 4.5357, -.9983,
5 -2.0712, 5.2088, -3.8337, .8331,
6 1.7130, .1390, -.1356, .0317,
7 .3626, -1.0206, .7242, -.1527,
8 -1.5767, 3.0242, -2.0075, .4169,
9 3.1870, -6.5555, 4.4847, -.9450,
C -2.3673, 4.6981, -3.1644, .6614/
DATA ALPB/
1 3.1773, -1.7469, .9801, -.1875,
2 -.2924, .1503, -.0395, .0040,
3 .8610, -2.1651, 1.5684, -.3370,
4 -1.2427, 2.7202, -1.8804, .3957/

```

```

IF (LCASE .EQ. 'T' .OR. LCASE .EQ. 't') L = 1
IF (LCASE .EQ. 'W' .OR. LCASE .EQ. 'w') L = 2
IF (LCASE .EQ. 'B' .OR. LCASE .EQ. 'b') L = 3
IF(L .LT. 1 .OR. L .GT. 3) PRINT *, 'LOAD TYPE NOT DEFINED'
IF(L .LT. 1 .OR. L .GT. 3) STOP
SCF = 0.0
Z2T = 2 * ZT
IF(L.LE.2) THEN
DO 11 I = 1, 4
I1 = I-1
IF (Z2T .EQ. 0.0) THEN
SCF = SCF + ALP(I,1,L) * RT**I1
ELSE
DO 10 J = 1, 5
J1 = (J-1)*2
SCF = SCF + ALP(I,J,L) * RT**I1 * Z2T**J1
10 CONTINUE
ENDIF
11 CONTINUE
ELSE
DO 20 I = 1, 4
I1 = I - 1
DO 20 J = 1, 4
J1 = 2*J - 1
SCF = SCF + ALPB(I,J) * RT**I1 * Z2T**J1
20 CONTINUE
ENDIF
RETURN
END
SUBROUTINE CSHANK(RT,BT,ZT,LCASE,SCF)

```

```

C-----
C
C THREE-DIMENSIONAL STRESS CONCENTRATION FACTOR FOR COUNTER-SUNK
C RIVET HOLE SUBJECTED TO:
C (1) REMOTE TENSION
C (2) REMOTE BENDING
C SOLUTION IS FOR THE COUNTER-SUNK ANGLE OF 100 DEGREES AND A
C SELECTED VALUE OF b/t (RATIOS ARE 0, .25, .50 AND 0.75).
C RESULTS FOR ANY OTHER b/t VALUE ARE COMPUTED BY LINEAR
C INTERPOLATION BETWEEN THE TWO LIMITING b/t VALUES.
C
C RANGE OF PARAMETERS: -0.5 < z/t < 0.5; 0.25 < r/t < 2.5
C
C-----
C
C DIMENSION ALP(3,5,4,2), BET(3,5,4,2)
C CHARACTER *1, LCASE

```

DATA ALP/

C 3.1675, 1.2562, -.4052, 3.7503, -8.8507, 2.8948, -15.6036,
 C 23.4071, -7.7898, 22.1981, -30.9691, 10.3670, -11.1465, 15.1933,
 C -5.0730, 3.5507, .7198, -.2232, .1185, 1.0574, -.2623,
 C -2.2035, 2.0077, -.4746, -4.2715, 5.0031, -1.4629, -2.9410,
 C 3.7985, -1.1888, 3.4454, .4835, -.1485, .3460, .1089,
 C .0844, -2.2150, 1.1287, -.0843, -6.5876, 7.3731, -2.1234,
 C -4.9136, 6.1237, -1.8862, 3.3341, .0777, -.0259, -.0229,
 C -.5498, .3049, -4.7184, 2.8236, -.5229, -12.1049, 12.3213,
 C -3.5036, -8.1604, 9.1806, -2.7318,
 C -2.7192, .4773, -.1620, 5.2713, 2.1888, -.6093, 3.2839,
 C -10.8632, 3.2768, -4.5453, 9.9384, -3.0428, .7327, -2.2565,
 C .7056, -1.4221, .4322, -.1424, 1.6817, -1.1265, .3481,
 C 1.2863, -2.0711, .6784, 2.4568, -3.8178, 1.2723, 1.8492,
 C -2.6911, .8911, .1935, -.0883, .0135, 3.8939, -2.7731,
 C .8887, 3.2128, -6.4904, 2.3056, 5.8885, -10.6559, 3.7525,
 C 3.9311, -6.2356, 2.1384, 1.7020, -.7146, .2021, 6.4706,
 C -4.6850, 1.4482, 8.3737, -12.5101, 4.0720, 14.4058, -19.9993,
 C 6.4740, 8.3649, -10.8222, 3.4552/

DATA BET/

C 3.1675, 1.2562, -.4052, 3.7503, -8.8507, 2.8948, -15.6036,
 C 23.4071, -7.7898, 22.1981, -30.9691, 10.3670, -11.1465, 15.1933,
 C -5.0730, 3.5507, .7198, -.2232, -1.4878, -4.1557, 1.2616,
 C .6958, 8.9708, -2.6866, 2.6002, -13.8774, 4.2240, -3.0363,
 C 8.2145, -2.5264, 3.4454, .4835, -.1485, -1.1969, -2.6156,
 C .7803, 1.0127, 1.8286, -.5102, .3438, -1.8037, .5698,
 C -1.3109, 1.7708, -.5768, 3.3341, .0777, -.0259, -.6655,
 C -1.7805, .5880, -.9018, 3.0805, -1.0493, 2.1386, -4.3757,
 C 1.5303, -1.6774, 2.7382, -.9445,
 C -2.7192, .4773, -.1620, 5.2713, 2.1888, -.6093, 3.2839,
 C -10.8632, 3.2768, -4.5453, 9.9384, -3.0428, .7327, -2.2565,
 C .7056, -1.4221, .4322, -.1424, 6.6870, -2.1064, .7330,
 C -9.2419, 4.3538, -1.5784, 13.6204, -9.2163, 3.1486, -7.6364,
 C 6.0611, -2.0053, .1935, -.0883, .0135, 2.8201, -1.4920,
 C .5510, -.4453, 1.8097, -.7420, .6186, -3.4144, 1.2552,
 C -1.1330, 2.6470, -.8987, 1.7020, -.7146, .2021, .2472,
 C -.4422, .2356, 1.8402, .0875, -.2380, -1.9081, -.4494,
 C .4036, .1992, .8738, -.3866/

C

C *** BEGIN ANALYSIS

C

IF (LCASE .EQ. 'T' .OR. LCASE .EQ. 't') L = 1
 IF (LCASE .EQ. 'B' .OR. LCASE .EQ. 'b') L = 2
 IF(L .LT. 1 .OR. L .GT. 2) PRINT *, 'LOAD TYPE NOT DEFINED'
 IF(L .LT. 1 .OR. L .GT. 2) STOP

```

IF(LCASE .EQ. 'W') PRINT *, 'WEDGE LOAD SOLUTION NOT AVAILABLE'
IF(LCASE .EQ. 'W') STOP
IF(BT .EQ. 0.0) K = 1
IF(BT .EQ. 0.25) K = 2
IF(BT .EQ. 0.50) K = 3
IF(BT .EQ. 0.75) K = 4
CCOR = (1. - 2*BT)/2.
SCF = 0.0
IF(BT .NE. 0.0) THEN
IF (-0.5 .LE. ZT .AND. ZT .LE. -CCOR) THEN
T1 = CCOR/BT
Z = T1 + ZT/BT
DO 11 I = 1, 3
I1 = I-1
IF( Z .EQ. 0.0) THEN
SCF = SCF + ALP(I,1,K,L) * RT**I1
ELSE
DO 10 J = 1, 5
J1 = J - 1
SCF = SCF + ALP(I,J,K,L) * RT**I1 * Z**J1
10 CONTINUE
ENDIF
11 CONTINUE
ELSE
T2 = CCOR/(1.-BT)
Z = T2 + ZT/(1.-BT)
DO 20 I = 1, 3
I1 = I-1
IF(Z .EQ. 0.0) THEN
SCF = SCF + BET(I,1,K,L) * RT**I1
ELSE
DO 21 J = 1, 5
J1 = J - 1
SCF = SCF + BET(I,J,K,L) * RT**I1 * Z**J1
21 CONTINUE
ENDIF
20 CONTINUE
ENDIF
ELSE
T2 = CCOR/(1.-BT)
Z = T2 + ZT/(1.-BT)
DO 30 I = 1, 3
I1 = I-1
IF(Z .EQ. 0.0) THEN
SCF = SCF + BET(I,1,K,L) * RT**I1
ELSE

```

```
DO 31 J = 1, 5
  J1 = J - 1
  SCF = SCF + BET(I,J,K,L) * RT**I1 * Z**J1
31  CONTINUE
    ENDIF
30  CONTINUE
    ENDIF
    RETURN
    END
```

References

1. Peterson, R. E.: *Stress Concentration Factors—Charts and Relations Useful in Making Strength Calculations for Machine Parts and Structural Elements*. John Wiley & Sons, Inc., c.1974.
2. Savin, G. N. (Eugene Gros, transl.): *Stress Concentration Around Holes*. Pergamon Press, Inc., 1961.
3. Green, A. E.: Three-Dimensional Stress Systems in Isotropic Plates. I. *Trans. Royal Soc. London*, ser. A, vol. 240, 1948, pp. 561-597.
4. Neuber, Heinz: *Theory of Notch Stresses: Principles for Exact Stress Calculation*. J. W. Edwards (Ann Arbor, Michigan), 1946.
5. Sternberg, E.; and Sadowsky, M. A.: Three-Dimensional Solution for the Stress Concentration Around a Circular Hole in a Plate of Arbitrary Thickness. *J. Appl. Mech.*, vol. 16, no. 1, Mar. 1949, pp. 27-38.
6. Folias, E. S.; and Wang, J.-J.: On the Three-Dimensional Stress Field Around a Circular Hole in a Plate of Arbitrary Thickness. *Comput. Mech.*, vol. 6, no. 3, 1990, pp. 379-391.
7. Love, A. E. H.: *A Treatise on the Mathematical Theory of Elasticity*, Fourth ed. Dover Publ., Inc., 1944.
8. Reissner, Eric: The Effect of Transverse Shear Deformation on the Bending of Elastic Plates. *J. Appl. Mech.*, vol. 12, no. 2, June 1945, pp. A-69-A-77.
9. Naghdi, P. M.: The Effect of Elliptic Holes on the Bending of Thick Plates. *J. Appl. Mech.*, vol. 22, no. 1, Mar. 1955, pp. 89-94.
10. Rubayi, N. A.; and Sosropartono, G. W.: Photoelastic Analysis of a Thick Plate With an Elliptical Hole Subjected to Simple Out-of-Plane Bending. *Exp. Mech.*, vol. 18, no. 9, Sept. 1978, pp. 335-343.
11. Goodier, J. N.: The Influence of Circular and Elliptical Holes on the Transverse Flexure of Elastic Plates. *Philos. Mag.*, ser. 7, vol. 22, no. 145, July 1936, pp. 69-80.
12. Goland, Martin: The Influence of the Shape and Rigidity of an Elastic Inclusion on the Transverse Flexure of Thin Plates. *J. Appl. Mech.*, vol. 10, no. 2, June 1943, pp. A-69-A-75.
13. Dumont, C.: *Stress Concentration Around an Open Circular Hole in a Plate Subjected to Bending Normal to the Plane of the Plate*. NACA TN 740, 1939.
14. Goodier, J. N.; and Lee, G. H.: An Extension of the Photoelastic Method of Stress Measurement to Plates in Transverse Bending. *J. Appl. Mech.*, vol. 8, no. 1, Mar. 1941, pp. A-27-A-29.
15. Drucker, D. C.: The Photoelastic Analysis of Transverse Bending of Plates in the Standard Transmission Polariscopes. *J. Appl. Mech.*, vol. 9, no. 4, Dec. 1942, pp. A-161-A-164.
16. Whaley, Richard E.: Stress-Concentration Factors for Countersunk Holes. *Exp. Mech.*, vol. 5, no. 8, Aug. 1965, pp. 257-261.
17. Cheng, Y. F.: Stress-Concentration Factors for a Countersunk Hole in a Flat Bar in Tension and Transverse Bending. *J. Appl. Mech.*, vol. 45, no. 4, Dec. 1978, pp. 929-932.
18. Bickley, W. G.: The Distribution of Stress Round a Circular Hole in a Plate. *Philos. Trans. Royal Soc. London*, ser. A, vol. 227, Aug. 1928, pp. 383-415.
19. Crews, John H., Jr.: A Survey of Strength Analysis Methods for Laminates With Holes. *J. Aeronaut. Soc. India*, vol. 36, no. 4, Nov. 1984, pp. 287-303.
20. Newman, J. C., Jr.: Finite-Element Analysis of Fatigue Crack Propagation—Including the Effects of Crack Closure. Ph.D. Thesis, Virginia Polytechnic Inst. and State Univ., May 1974.
21. Shivakumar, K. N.; and Raju, I. S.: Treatment of Singularities in Cracked Bodies. *Int. J. Fract.*, vol. 45, no. 3, Oct. 1, 1990, pp. 159-178.
22. Sih, G. C.: A Review of the Three-Dimensional Stress Problem for a Cracked Plate. *Int. J. Fract. Mech.*, vol. 7, no. 1, Mar. 1971, pp. 39-61.
23. Businger, Peter; and Golub, Gene H.: Linear Least Squares Solutions by Householder Transformations. *Numer. Math.*, Bd. 7, Heft 3, 1965, pp. 269-276.
24. Chang, Fu-Kuo; Scott, Richard A.; and Springer, George S.: Strength of Mechanically Fastened Composite Joints. *J. Compos. Mater.*, vol. 16, no. 6, Nov. 1982, pp. 470-494.
25. Crews, John H., Jr.; Hong, C. S.; and Raju, I. S.: *Stress-Concentration Factors for Finite Orthotropic Laminates With a Pin-Loaded Hole*. NASA TP-1862, 1981.
26. DeJong, Theo: Stresses Around Pin-Loaded Holes in Elastically Orthotropic or Isotropic Plates. *J. Compos. Mater.*, vol. 11, July 1977, pp. 313-331.
27. Eshwar, V. A.; Dattaguru, B.; and Rao, A. K.: *Partial Contact and Friction in Pin Joints*. Rep. No. ARDB-STR-5010, Dep. of Aeronautical Engineering, Indian Inst. of Science, Dec. 1977.

Table 1. Details of Finite-Element Idealization of Plates With Countersunk Holes

b/t	Nodes	Elements	Number of layers	Layer of thickness as percentage of plate thickness ^a
0	5756	1170	9	2, 5, 15, 15, 26, 15, 15, 5, 2
.25	6938	1430	11	2, 5, 11, 5, 2, 2, 5, 15, 40, 9, 4
.50	7529	1560	12	3, 8, 17, 15, 5, 2, 2, 5, 15, 17, 8, 3
.75	6938	1430	11	4, 9, 40, 15, 5, 2, 2, 5, 11, 5, 2

^aLayers are numbered from $z/t = -0.5$ plane.

Table 2. Comparison of Stress-Concentration Factors for Countersunk Holes in Plates
 $[b/t = 0.6; \theta_c = 90^\circ]$

Load	r/t	w/r	t/r	z/t	Stress-concentration factor from	
					Cheng (ref. 17)	Present
Tension (model 7)	0.24	7.2	7.2	0.1	4.19	^a 4.310
Bending (model 8)	0.19	8.2	8.2	-0.50	-2.61	^b -2.510
	.19	8.2	8.2	.10	1.08	2.216
	.19	8.2	8.2	.50	2.00	1.689

^a $K_{t_{\max}} = 4.37$ at $z/t = 0.08$.

^b $K_{b_{\max}} = -2.55$ at $z/t = -0.48$.

Table 3. Coefficients of K_t Equation for Straight-Shank Hole in Plate Subjected to Remote Tension

i	α_{ij} for j of--				
	0	2	4	6	8
0	3.1825	0.4096	-1.2831	2.2778	-2.0712
1	.1679	-1.1525	2.8632	-6.0148	5.2088
2	-.2063	1.1650	-2.0000	4.5357	-3.8337
3	.0518	-.2539	.4239	-.9983	.8331

Table 4. Coefficients of K_w Equation for Straight-Shank Hole in Plate Subjected to Wedge Loading

i	α_{ij} for j of--				
	0	2	4	6	8
0	1.7130	0.3626	-1.5767	3.1870	-2.3673
1	.1390	-1.0206	3.0242	-6.5555	4.6981
2	-.1356	.7242	-2.0075	4.4847	-3.1644
3	.0317	-.1527	.4169	-.9450	.6614

Table 5. Coefficients of K_b Equation for Straight-Shank Hole in Plate Subjected to Remote Bending

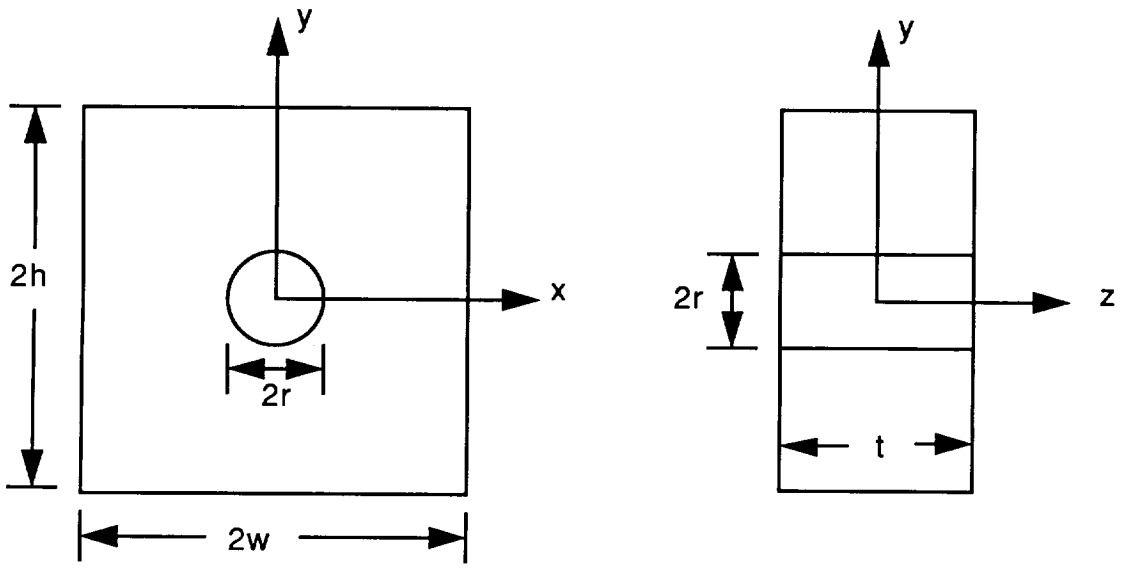
i	α_{ij} for j of--			
	1	3	5	7
0	3.1773	0.2924	0.8610	-1.2427
1	-1.7469	.1503	-2.1651	2.7202
2	.9801	-.0395	1.5684	-1.8804
3	-.1875	.0040	-.3370	.3957

Table 6. Coefficients of K_I Equation for Countersunk Hole in Plate Subjected to Remote Tension Stress S

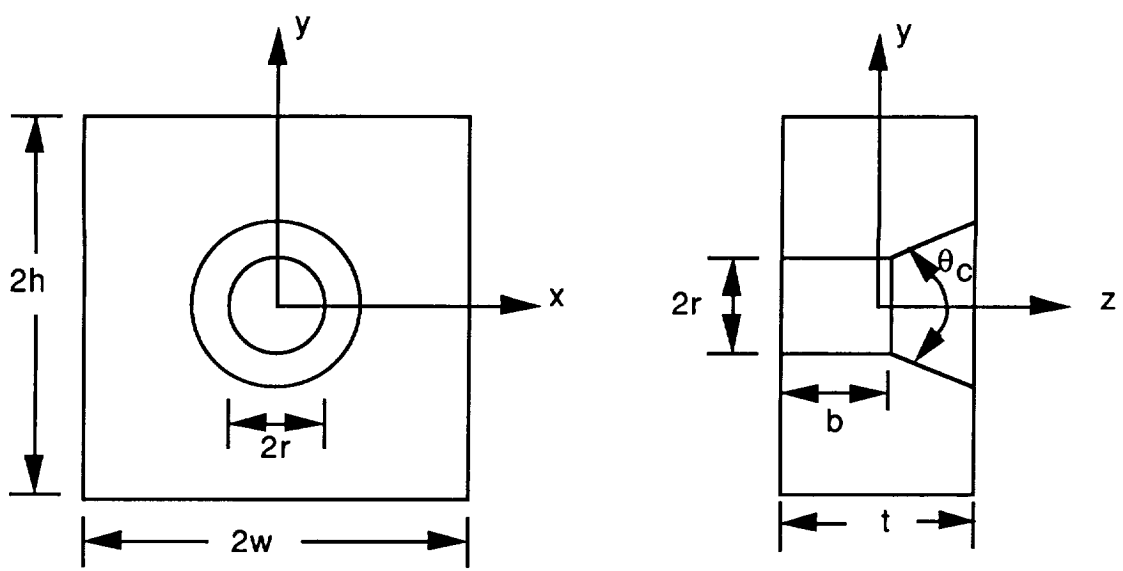
b/t	i	α_{ij} for $-0.5 \leq z/t \leq -(0.5 - b/t)$ and j of					β_{ij} for $-(0.5 - b/t) \leq z/t \leq 0.5$ and j of				
		0	1	2	3	4	0	1	2	3	4
0	0	3.1675	3.7503	-15.6036	22.1981	-11.1465	3.1675	3.7503	-15.6036	22.1981	-11.1465
	1	1.2562	-8.8507	23.4071	-30.9691	15.1933	1.2562	-8.8507	23.4071	-30.9691	15.1933
	2	-.4052	2.8948	-7.7898	10.3670	-5.0730	-.4052	2.8948	-7.7898	10.3670	-5.0730
0.25	0	3.5507	0.1185	-2.2035	-4.2715	-2.9410	3.5507	-1.4878	0.6958	2.6002	-3.0363
	1	.7198	1.0574	2.0077	5.0031	3.7985	.7198	-4.1557	8.9708	-13.8774	8.2145
	2	-.2232	-.2623	-.4746	-1.4629	-1.1888	-.2232	1.2616	-2.6866	4.2240	-2.5264
0.50	0	3.4454	0.3460	-2.2150	-6.5876	-4.9136	3.4454	-1.1969	1.0127	0.3438	-1.3109
	1	.4835	.1089	1.1287	7.3731	6.1237	.4835	-2.6156	1.8286	-1.8037	1.7708
	2	-.1485	.0844	-.0843	-2.1234	-1.8862	-.1485	.7803	-.5102	.5698	-.5768
0.75	0	3.3341	-0.0029	-4.7184	-12.1049	-8.1604	3.3341	-0.6655	-0.9018	2.1386	-1.6774
	1	.0777	-.5498	2.8236	12.3213	9.1806	.0777	-1.7805	3.0805	-4.3757	2.7382
	2	-.0259	.3049	-.5229	-3.5036	-2.7318	-.0259	.5880	-1.0493	1.5303	-.9445

Table 7. Coefficients of K_{II} Equation for Countersunk Hole in Plate Subjected to Unit Bending Stress

b/t	i	α_{ij} for $-0.5 \leq z/t \leq -(0.5 - b/t)$ and j of					β_{ij} for $-(0.5 - b/t) \leq z/t \leq 0.5$ and j of				
		0	1	2	3	4	0	1	2	3	4
0	0	-2.7192	5.2713	3.2839	-4.5453	0.7327	-2.7192	5.2713	3.2839	-4.5453	0.7327
	1	.4773	2.1888	-10.8632	9.9384	-2.2565	.4773	2.1888	-10.8632	9.9384	-2.2565
	2	-.1620	-.6093	3.2768	-3.0428	.7056	-.1620	-.6093	3.2768	-3.0428	.7056
0.25	0	-1.4221	1.6817	1.2863	2.4568	1.8492	-1.4221	6.6870	-9.2419	13.6204	-7.6364
	1	.4322	-1.1265	-2.0711	-3.8178	-2.6911	.4322	-2.1064	4.3538	-9.2163	6.0611
	2	-.1424	.3481	.6784	1.2723	.8911	-.1424	.7330	-1.5784	3.1486	-2.0053
0.50	0	0.1935	3.8939	3.2128	5.8885	3.9311	0.1935	2.8201	-0.4453	0.6186	-1.1330
	1	-.0883	-2.7731	-6.4904	-10.6559	-6.2356	-.0883	-1.4920	1.8097	-3.4144	2.6470
	2	.0135	.8887	2.3056	3.7525	2.1384	.0135	.5510	-.7420	1.2552	-.8987
0.75	0	1.7020	6.4706	8.3737	14.4058	8.3649	1.7020	0.2472	1.8402	-1.9081	0.1992
	1	-.7146	-4.6850	-12.5101	-19.9993	-10.8222	-.7146	-.4422	.0875	-.4494	.8738
	2	.2021	1.4482	4.0720	6.4740	3.4552	.2021	.2356	-.2380	.4036	-.3866

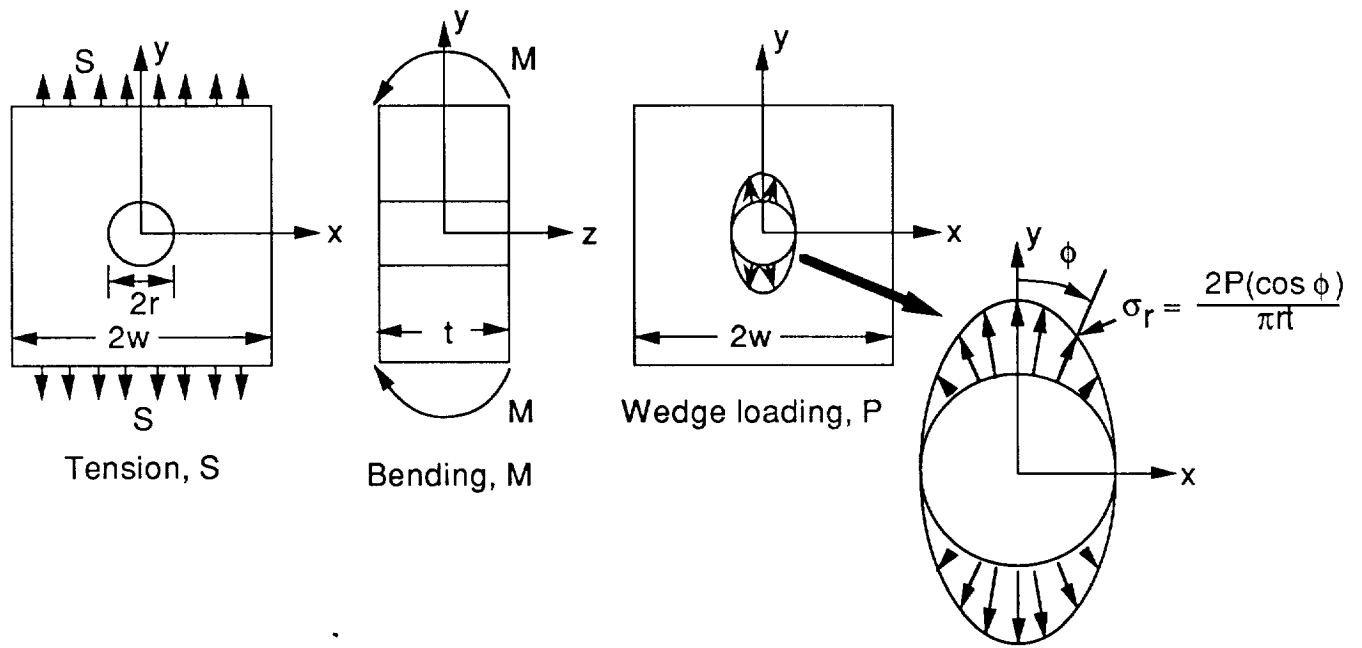


(a) Straight-shank rivet hole.

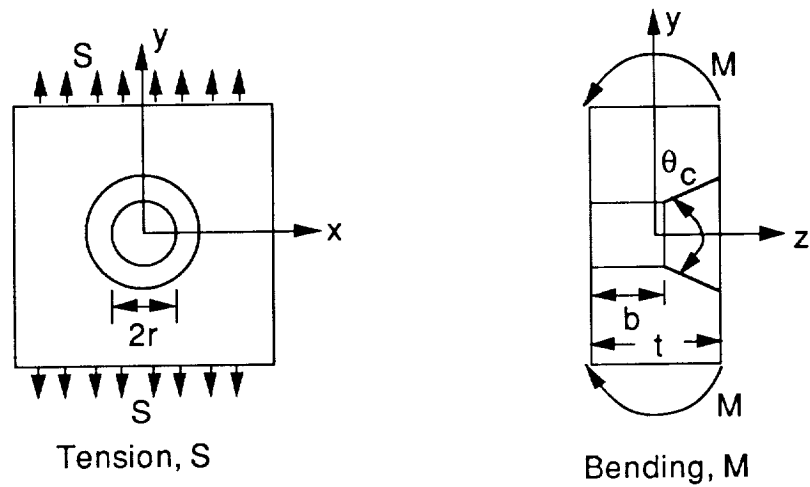


(b) Countersunk rivet hole.

Figure 1. Nomenclature and configurations of straight-shank and countersunk rivet holes.

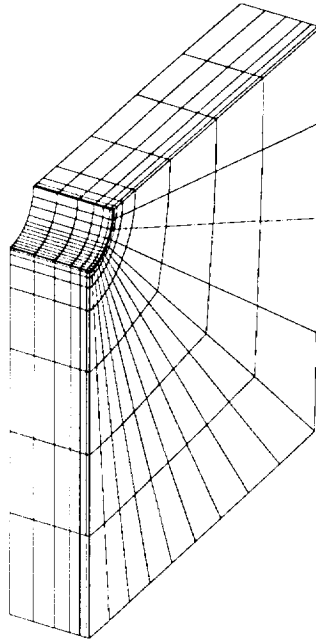


(a) Loading on straight-shank hole.

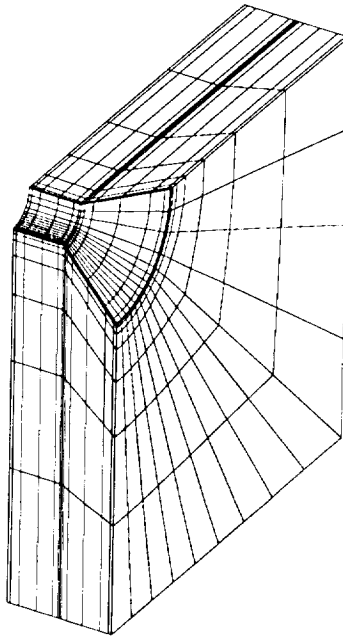


(b) Loading on countersunk hole.

Figure 2. Types of loading on straight-shank and countersunk holes in plates.



(a) Straight-shank hole; $r/t = 1$.



(b) Countersunk hole; $r/t = 0.25$; $b/t = 0.50$; $\theta_c = 100^\circ$.

Figure 3. Typical finite-element models for plates with straight-shank and countersunk holes.

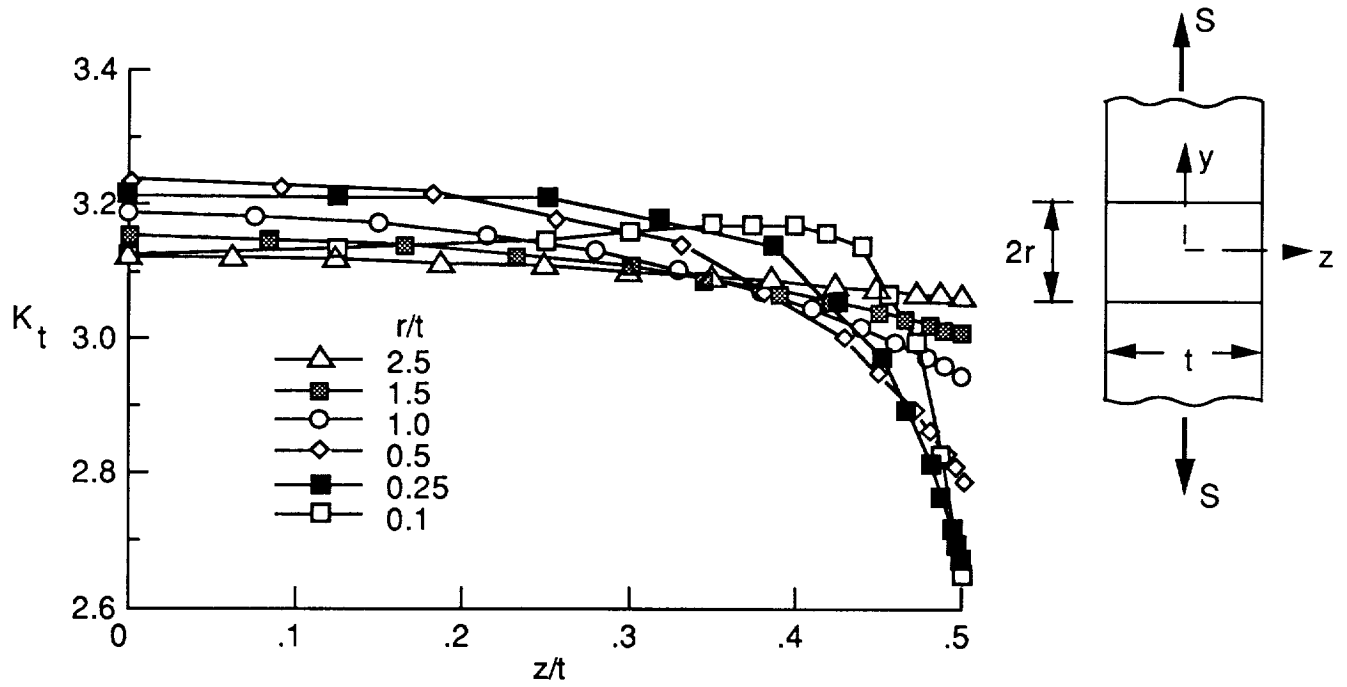


Figure 4. Three-dimensional tension stress-concentration factor distribution along bore of straight-shank holes. $w/r = h/r = 5$.

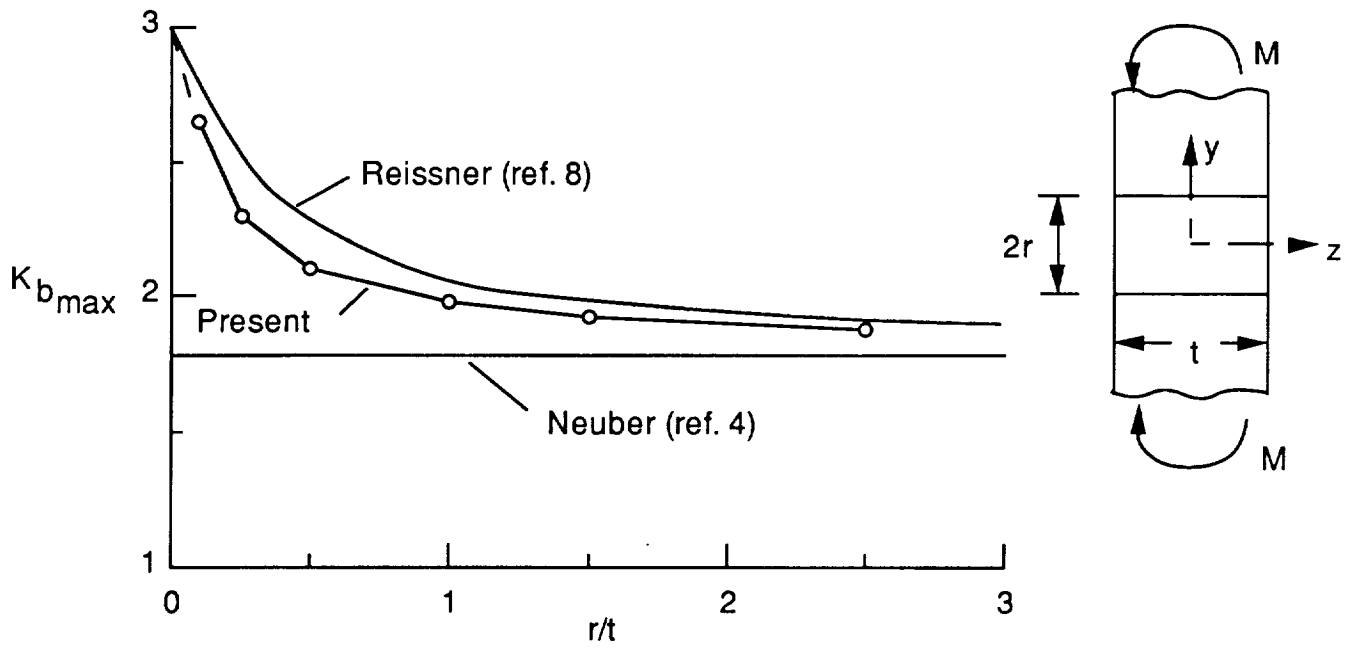
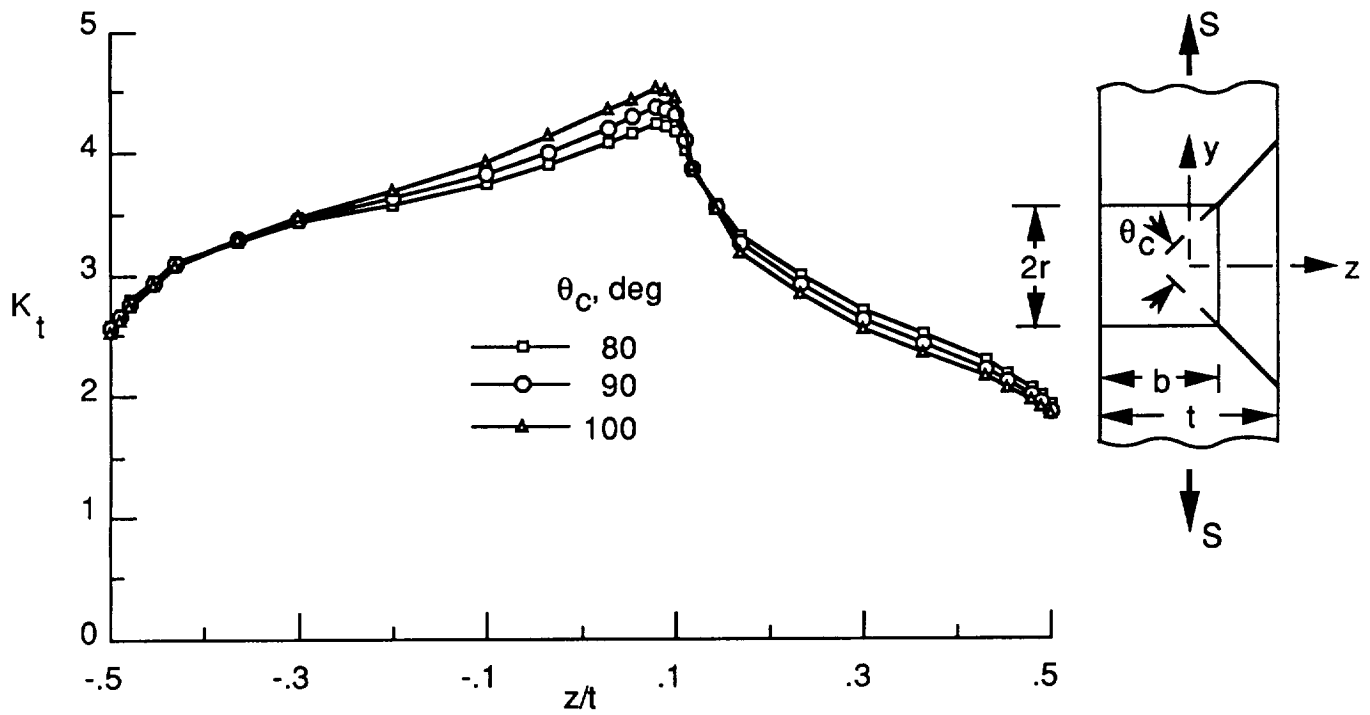
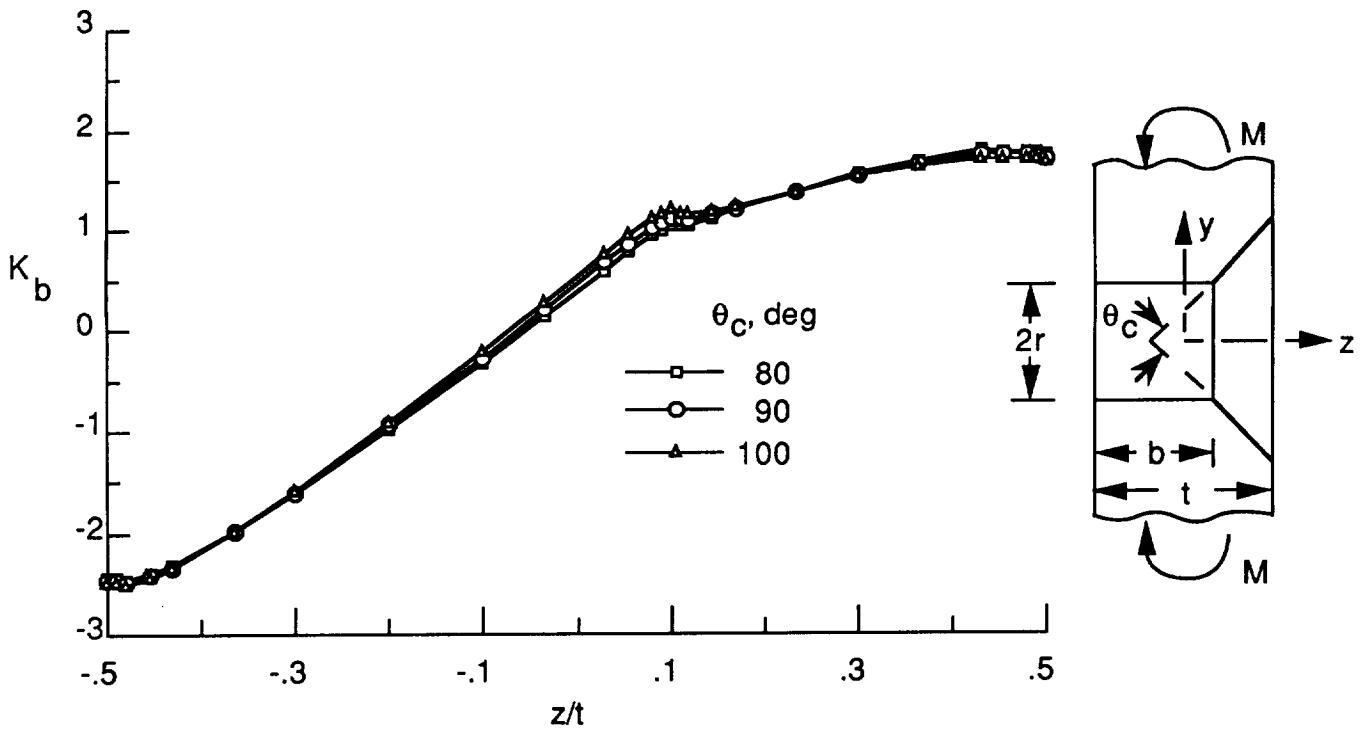


Figure 5. Comparison of maximum bending stress-concentration factor from various analyses. $w/r = h/r = 5$.

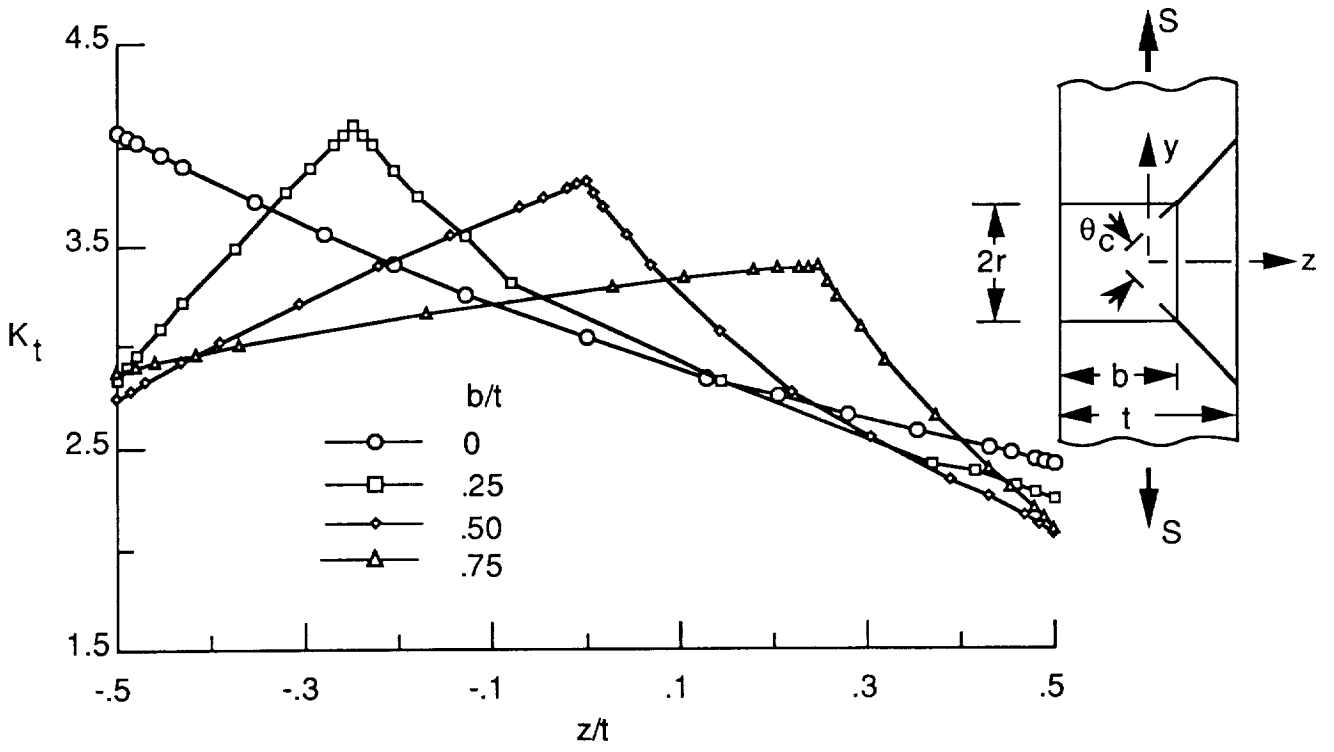


(a) Tension stress-concentration factor.

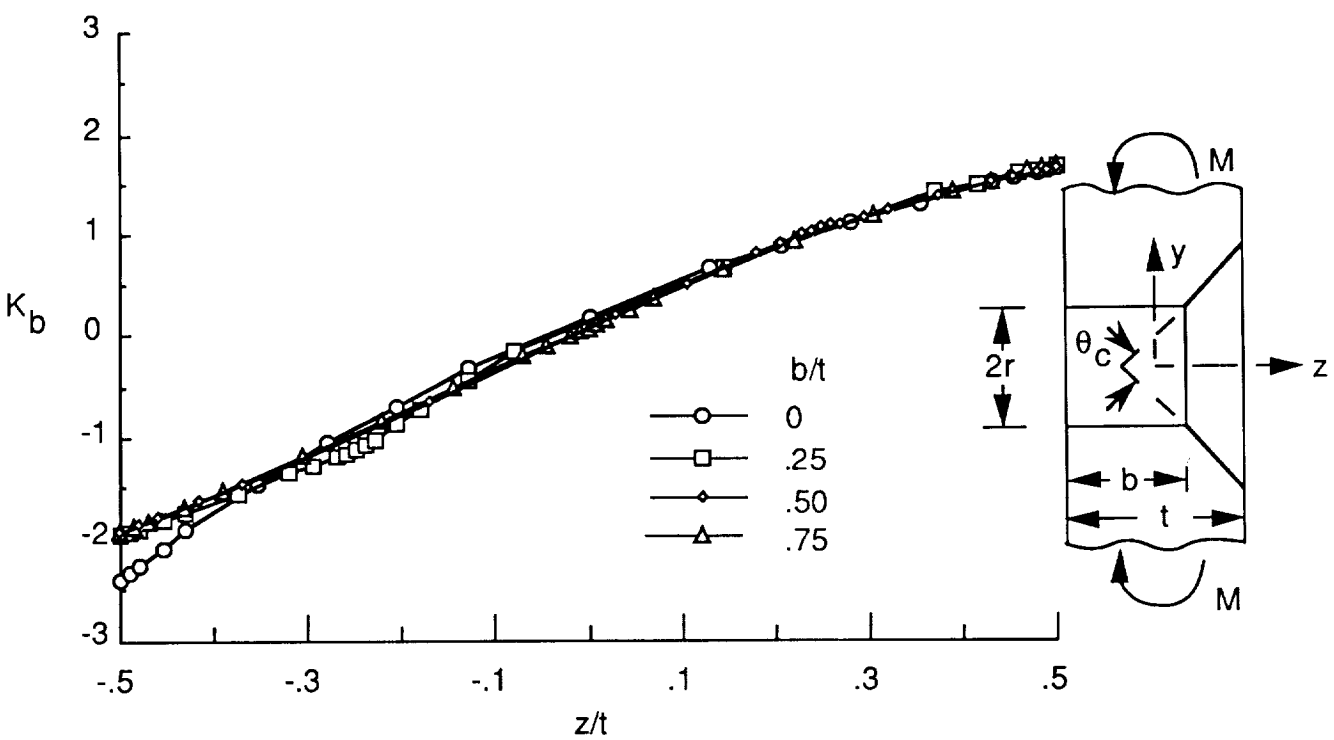


(b) Bending stress-concentration factor.

Figure 6. Effect of countersink angle θ_c on tension and bending stress-concentration factor for countersunk holes in plates. $r = 1.0$; $r/t = 0.24$; $w/r = 7.2$; $h/r = 7.2$; $b/t = 0.6$.



(a) Tension stress-concentration factor.



(b) Bending stress-concentration factor.

Figure 7. Effect of b/t on stress-concentration factors in countersunk holes in plates. $r/t = 2.0$; $w/r = 7.5$; $h/r = 7.5$; $\theta_c = 100^\circ$.

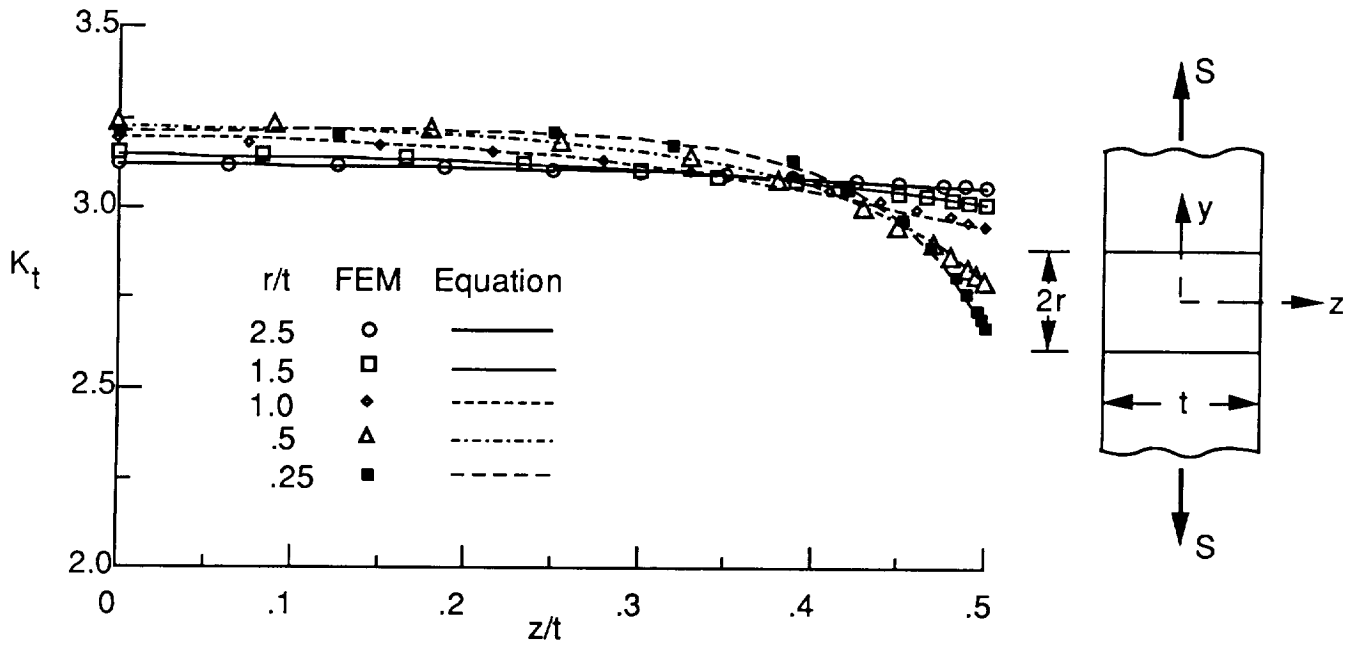


Figure 8. Comparison of tension SCF equation results with F-E results for straight-shank holes.

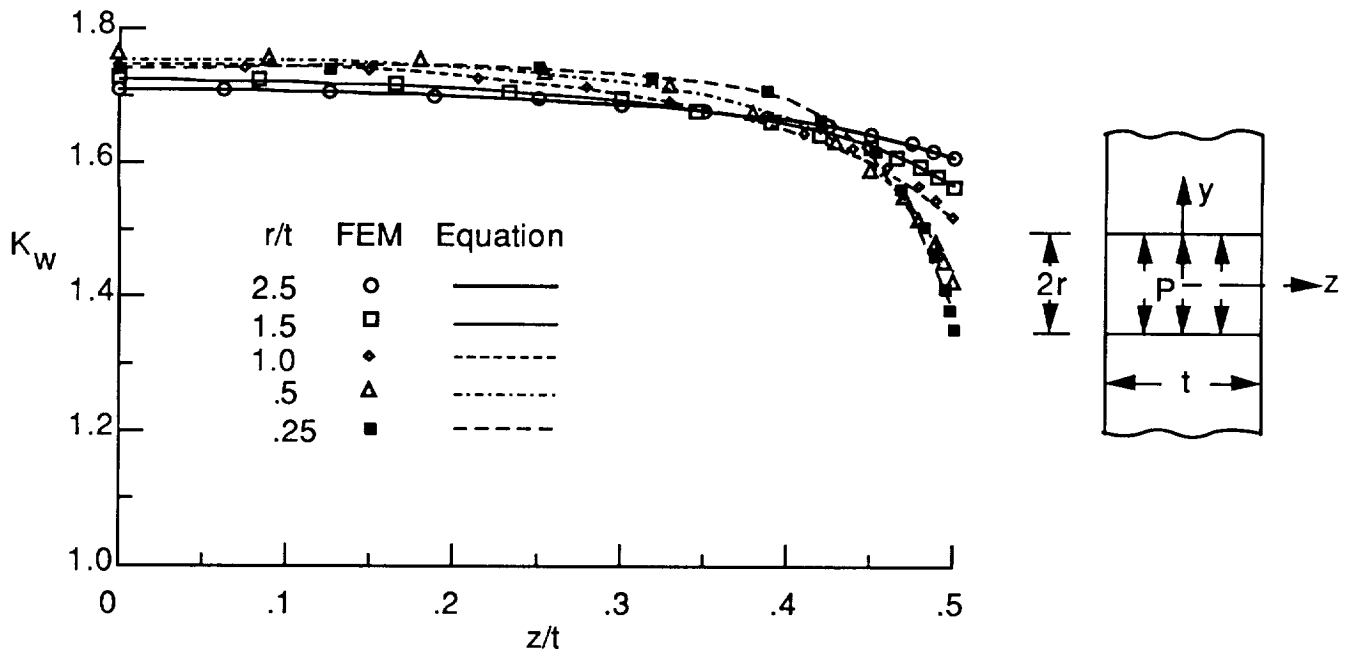


Figure 9. Comparison of wedge loading SCF equation results with F-E results for straight-shank holes.

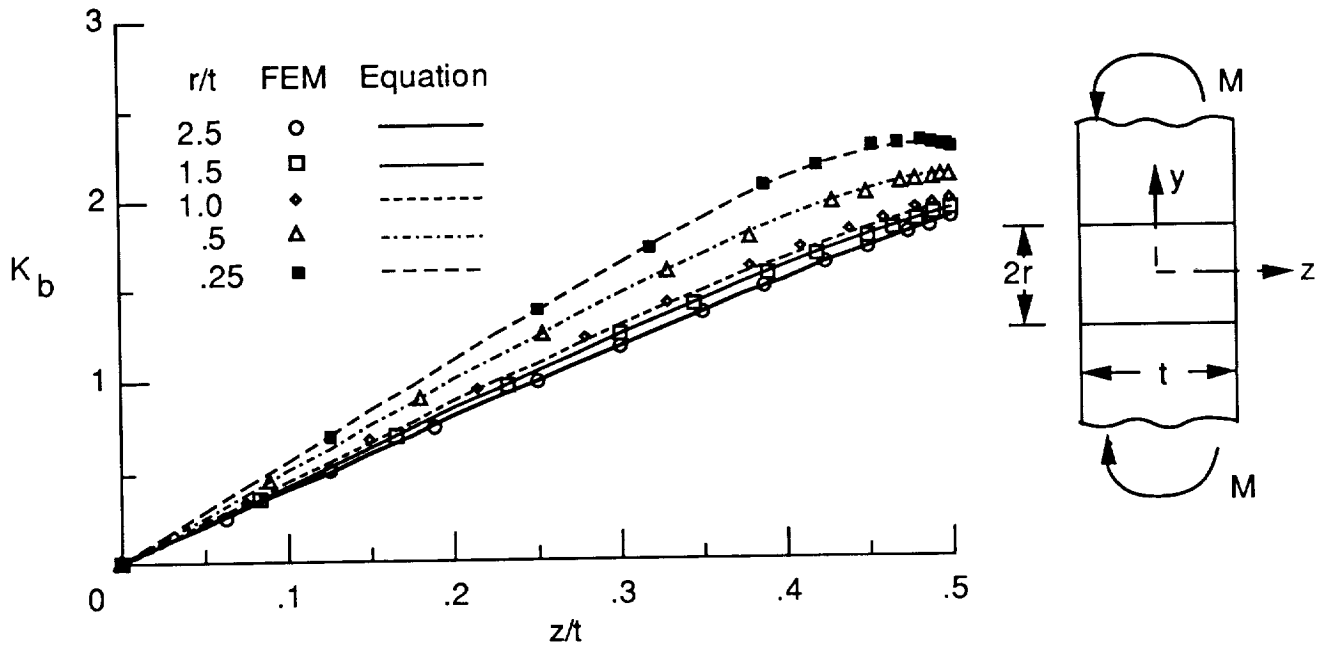


Figure 10. Comparison of bending SCF equation results with F-E results for straight-shank holes.

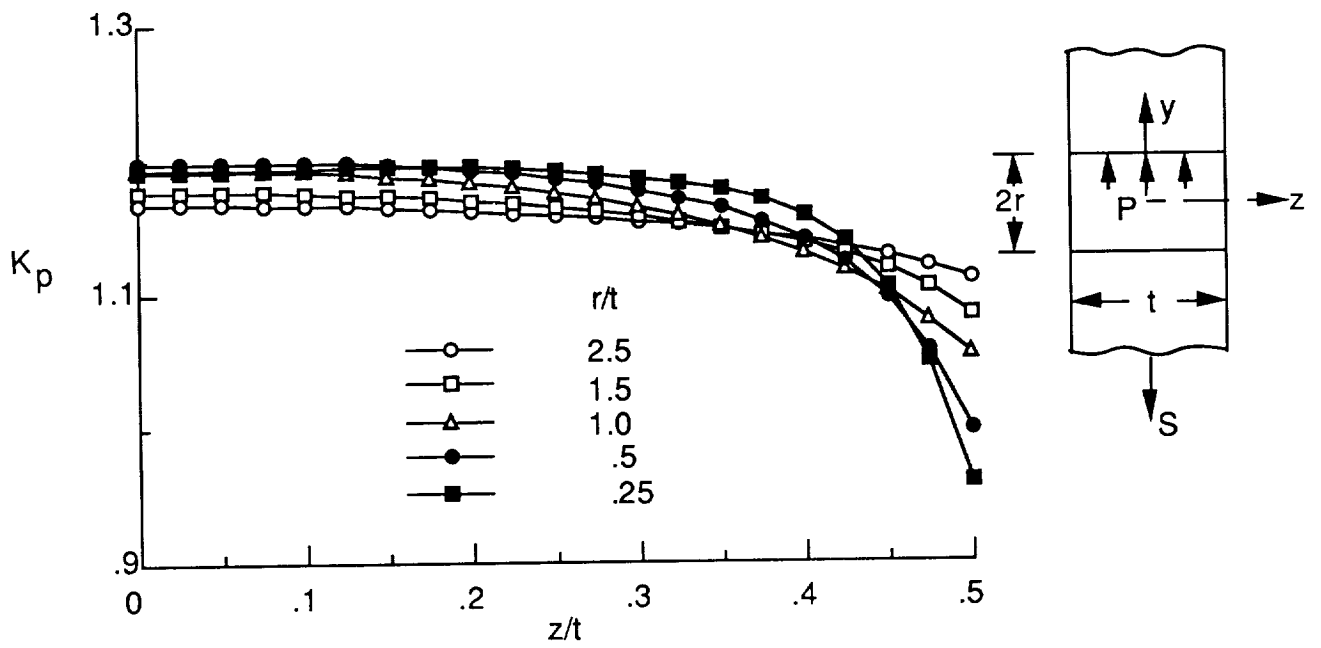
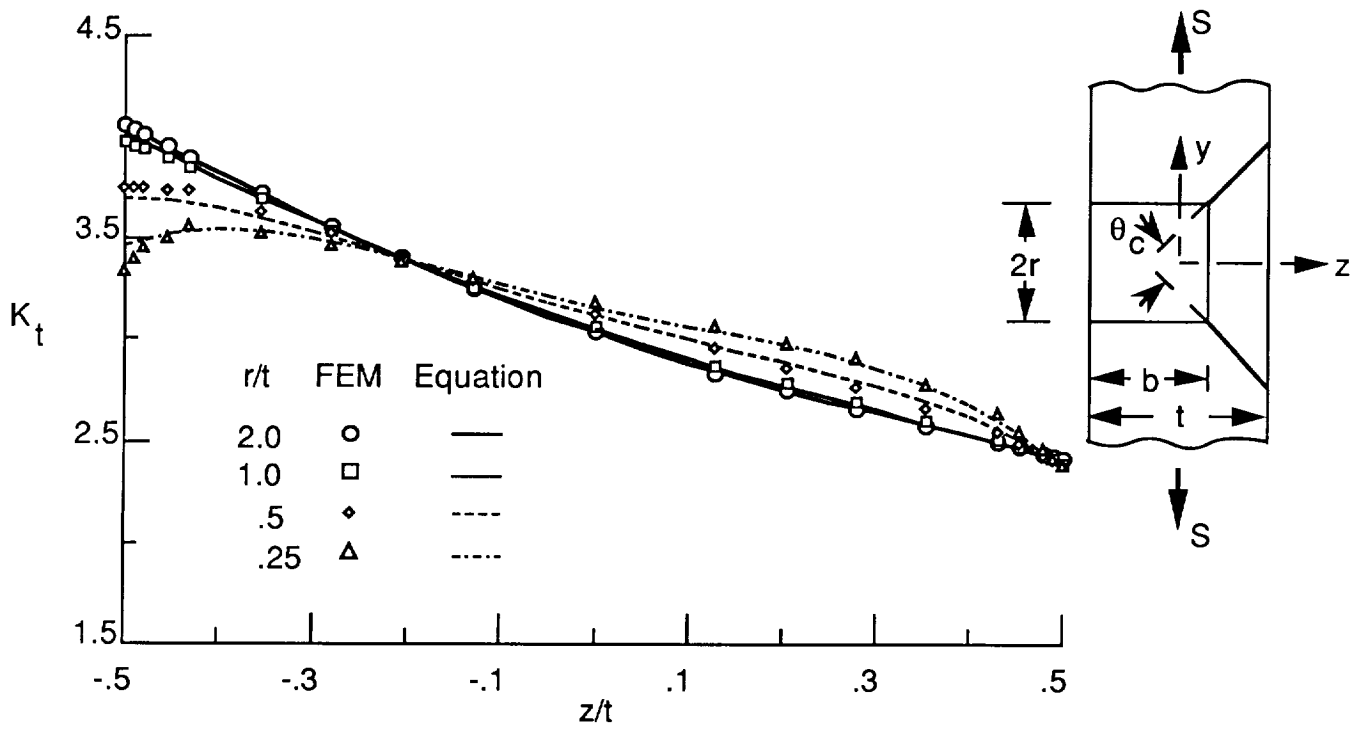
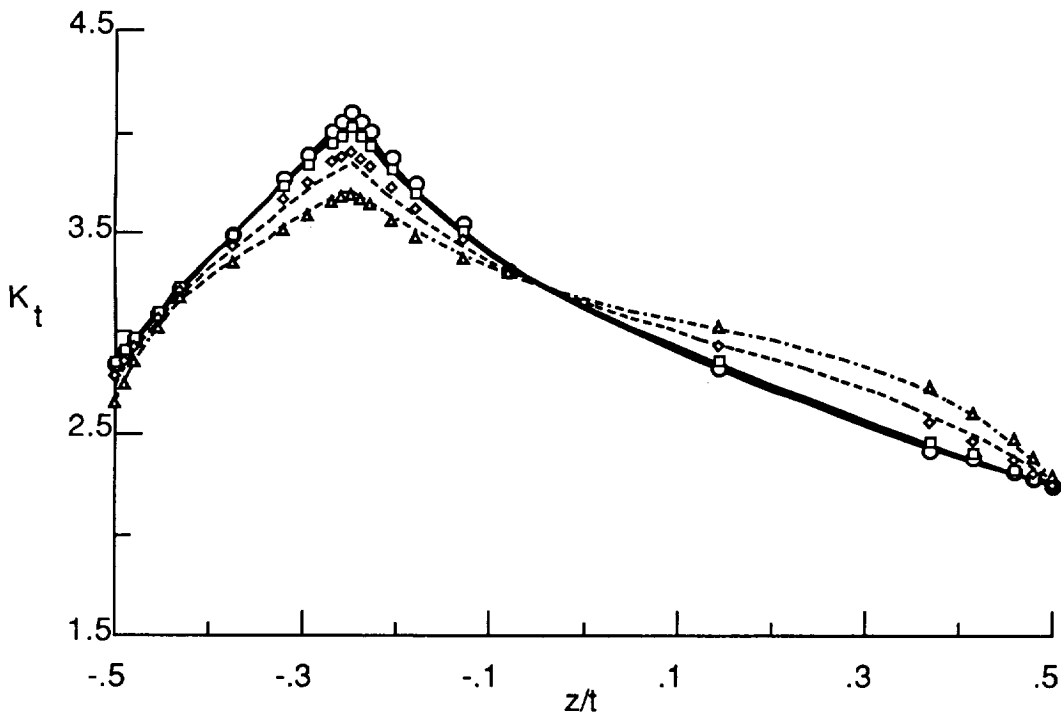


Figure 11. Three-dimensional SCF for pin-loaded plates with straight-shank holes.

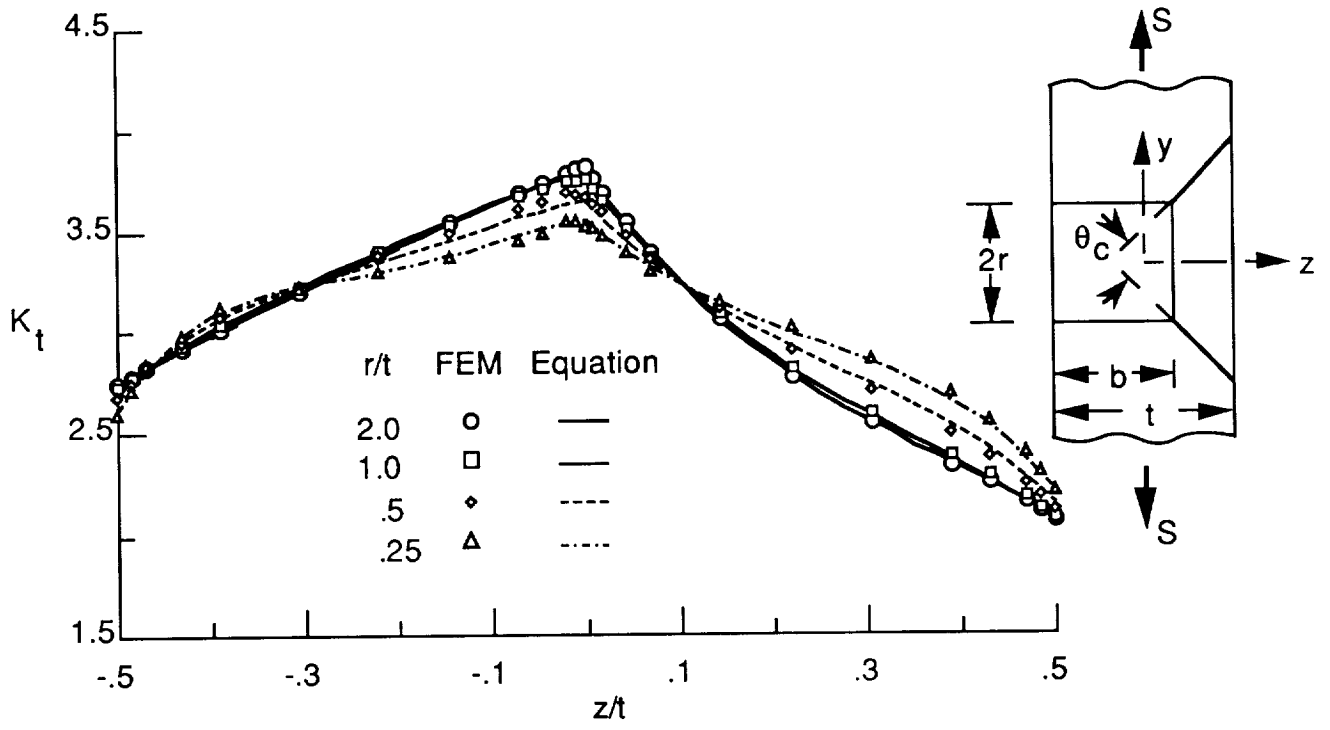


(a) $b/t = 0$; $\theta_c = 100^\circ$.

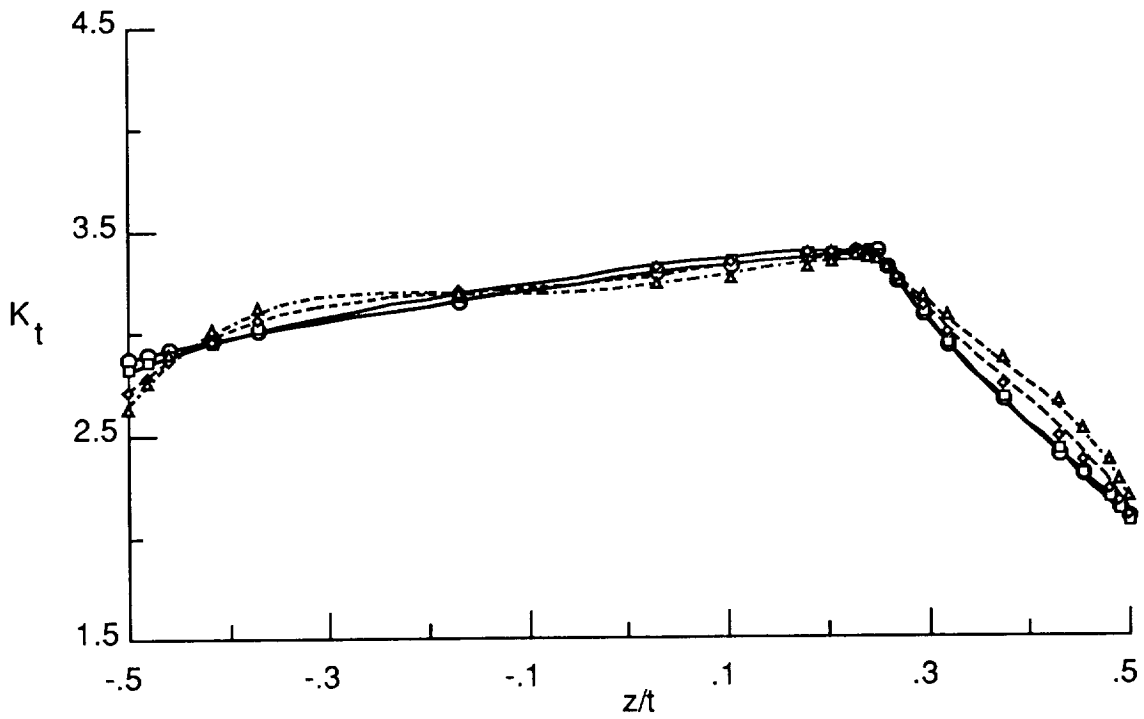


(b) $b/t = 0.25$; $\theta_c = 100^\circ$.

Figure 12. Comparison of tension SCF equation results with F-E results for countersunk holes.

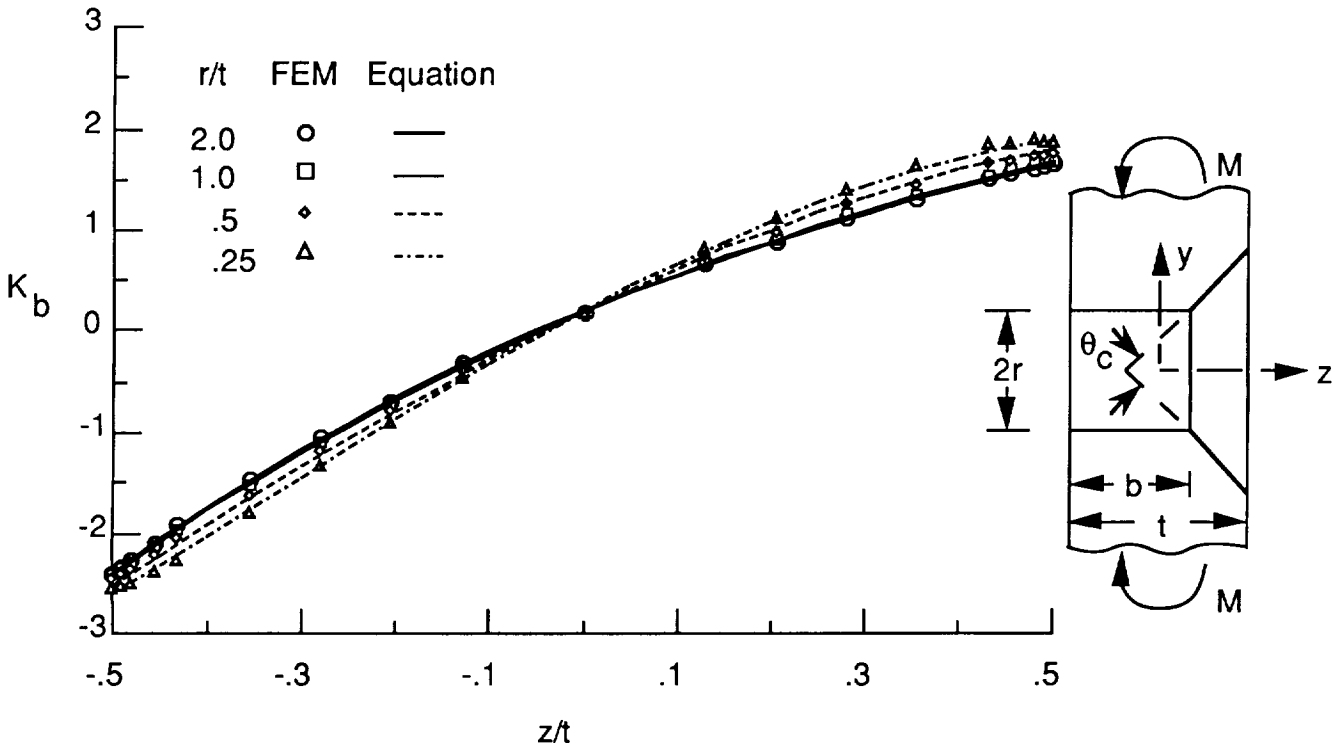


(c) $b/t = 0.50$; $\theta_c = 100^\circ$.

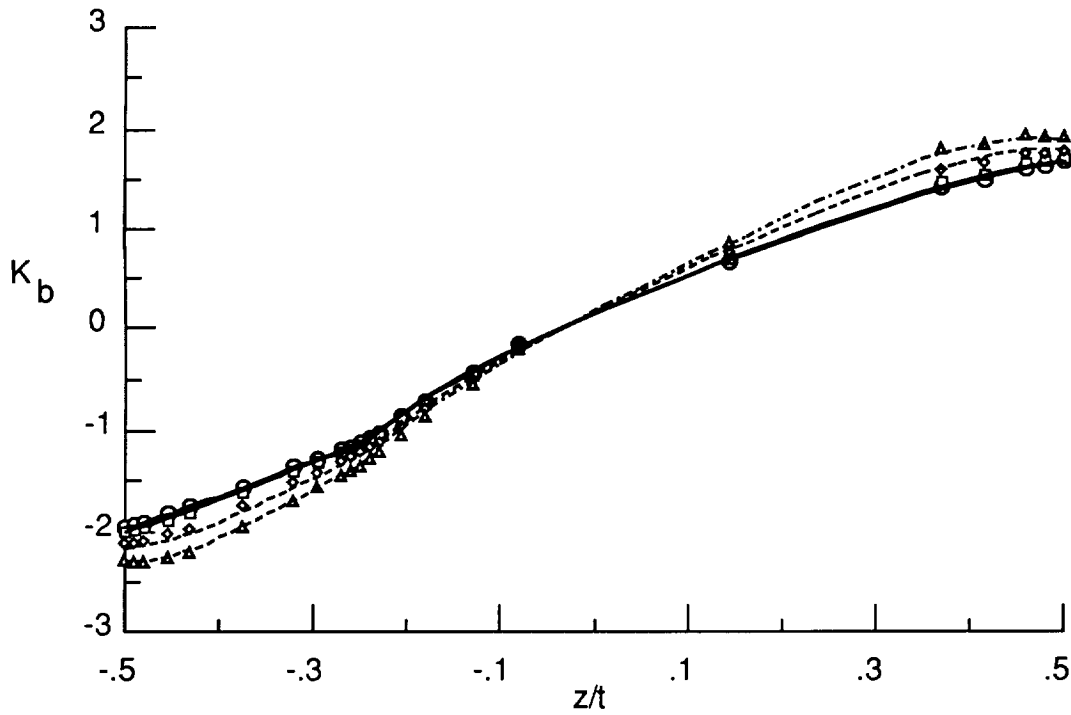


(d) $b/t = 0.75$; $\theta_c = 100^\circ$.

Figure 12. Concluded.

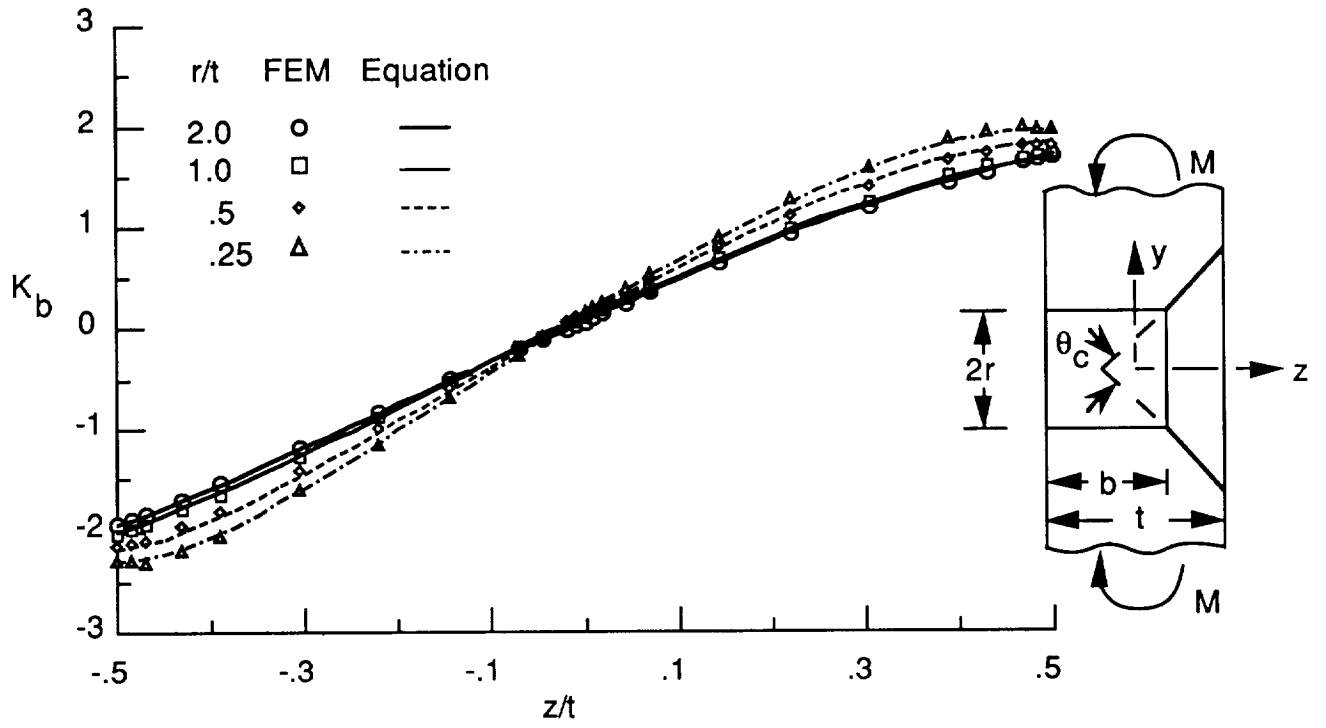


(a) $b/t = 0$; $\theta_c = 100^\circ$.

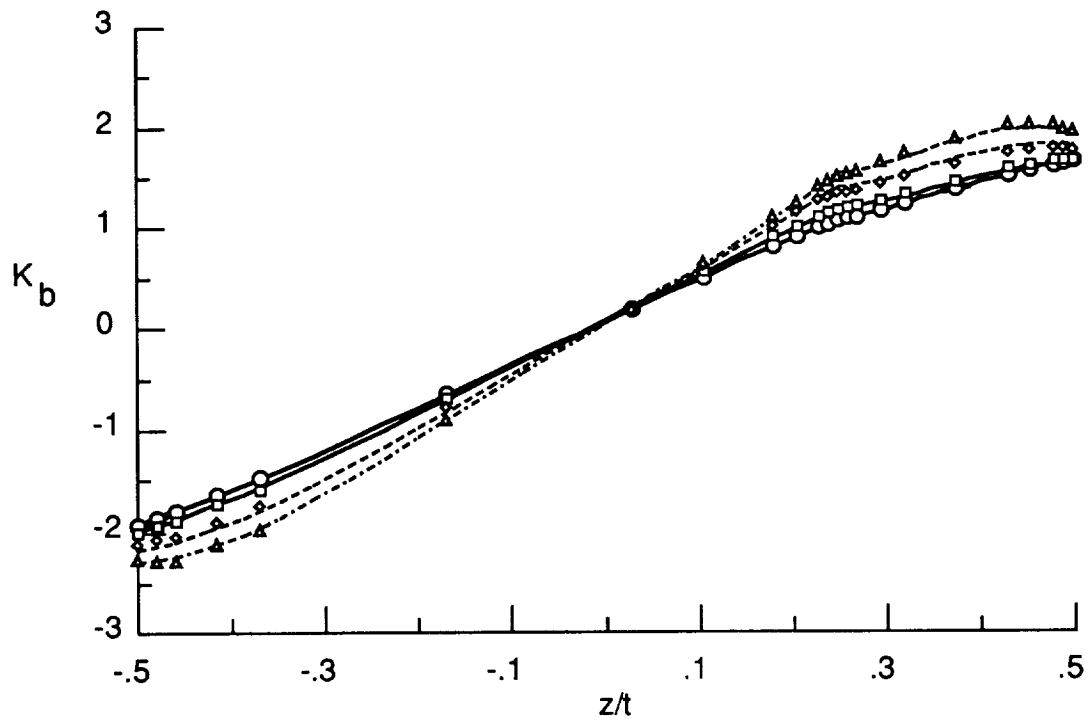


(b) $b/t = 0.25$; $\theta_c = 100^\circ$.

Figure 13. Comparison of bending SCF equation results with F-E results for countersunk holes.

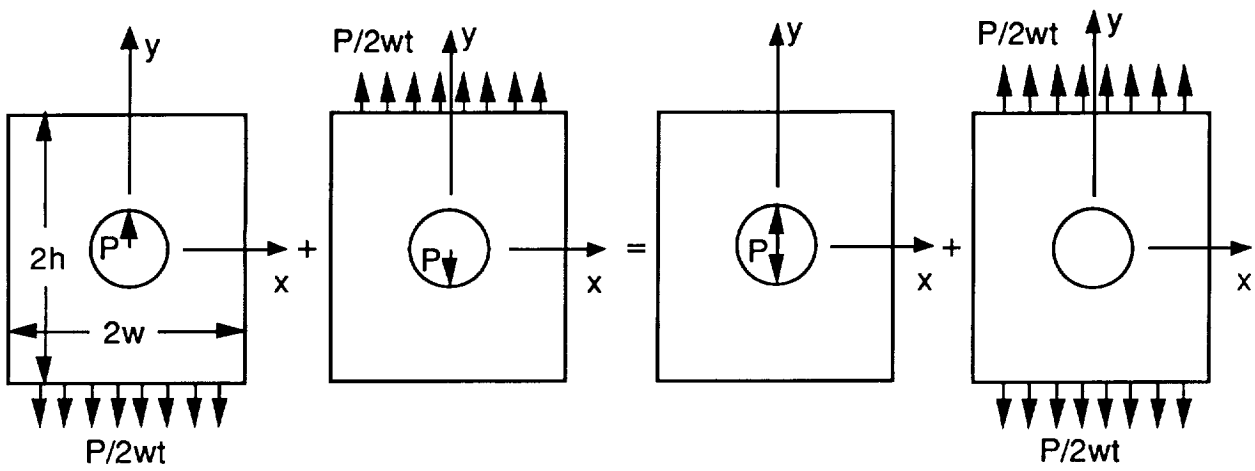


(c) $b/t = 0.50$; $\theta_c = 100^\circ$.



(d) $b/t = 0.75$; $\theta_c = 100^\circ$.

Figure 13. Concluded.



(a) Pin loading. (b) Pin loading. (c) Wedge loading. (d) Tension.

Figure 14. Superposition of wedge loading and remote tension solutions to calculate pin-load SCF.

REPORT DOCUMENTATION PAGE			Form Approved OMB No. 0704-0188	
Public reporting burden for this collection of information is estimated to average 1 hour per response, including the time for reviewing instructions, searching existing data sources, gathering and maintaining the data needed, and completing and reviewing the collection of information. Send comments regarding this burden estimate or any other aspect of this collection of information, including suggestions for reducing this burden, to Washington Headquarters Services, Directorate for Information Operations and Reports, 1215 Jefferson Davis Highway, Suite 1204, Arlington, VA 22202-4302, and to the Office of Management and Budget, Paperwork Reduction Project (0704-0188), Washington, DC 20503.				
1. AGENCY USE ONLY (Leave blank)	2. REPORT DATE June 1992	3. REPORT TYPE AND DATES COVERED Technical Paper		
4. TITLE AND SUBTITLE Stress Concentrations for Straight-Shank and Countersunk Holes in Plates Subjected to Tension, Bending, and Pin Loading			5. FUNDING NUMBERS WU 505-63-50-04	
6. AUTHOR(S) K. N. Shivakumar and J. C. Newman, Jr.				
7. PERFORMING ORGANIZATION NAME(S) AND ADDRESS(ES) NASA Langley Research Center Hampton, VA 23665-5225			8. PERFORMING ORGANIZATION REPORT NUMBER L-17027	
9. SPONSORING/MONITORING AGENCY NAME(S) AND ADDRESS(ES) National Aeronautics and Space Administration Washington, DC 20546-0001			10. SPONSORING/MONITORING AGENCY REPORT NUMBER NASA TP-3192	
11. SUPPLEMENTARY NOTES Shivakumar: Analytical Services & Materials, Inc., Hampton, VA; Newman: Langley Research Center, Hampton, VA.				
12a. DISTRIBUTION/AVAILABILITY STATEMENT Unclassified--Unlimited Subject Category 39			12b. DISTRIBUTION CODE	
13. ABSTRACT (Maximum 200 words) A three-dimensional stress-concentration analysis was conducted on straight-shank and countersunk (rivet) holes in a large plate subjected to various loading conditions. Three-dimensional finite-element analyses were performed with 20-node isoparametric elements. The plate material was assumed to be linear elastic and isotropic, with a Poisson's ratio of 0.3. Stress concentrations along the bore of the hole were computed for several ratios of hole radius to plate thickness (0.1 to 2.5) and ratios of countersink depth to plate thickness (0.25 to 1). The countersink angle was varied from 80° to 100° in some typical cases, but the angle was held constant at 100° for most cases. For straight-shank holes, three types of loading were considered: remote tension, remote bending, and wedge loading in the hole. Results for remote tension and wedge loading were used to estimate stress concentrations for simulated rivet or pin loading. For countersunk holes, only remote tension and bending were considered. Based on the finite-element results, stress-concentration equations were developed. Whenever possible, the present results were compared with other numerical solutions and experimental results from the literature.				
14. SUBJECT TERMS Countersunk holes; 3-D stress-concentration analysis; Finite-element analysis; Countersink angle; Isoparametric elements			15. NUMBER OF PAGES 34	
			16. PRICE CODE A03	
17. SECURITY CLASSIFICATION OF REPORT Unclassified	18. SECURITY CLASSIFICATION OF THIS PAGE Unclassified	19. SECURITY CLASSIFICATION OF ABSTRACT	20. LIMITATION OF ABSTRACT	